Atmos. Chem. Phys. Discuss., 12, 11765–11822, 2012
www.atmos-chem-phys-discuss.net/12/11765/2012/
doi:10.5194/acpd-12-11765-2012


Atmospheric Chemistry and Physics Discussions



# Formation and growth of nucleated particles: observational constraints on cloud condensation nuclei budgets

**D. M. Westervelt**[1], **I. Riipinen**[1,2,*], **J. R. Pierce**[3], **W. Trivitayanurak**[4], and **P. J. Adams**[1]

[1]Center for Atmospheric Particle Studies (CAPS), Carnegie Mellon Univ., Pittsburgh, PA, USA
[2]Department of Physics, University of Helsinki, Helsinki, Finland
[3]Department of Physics and Atmospheric Science, Dalhousie University, Halifax, NS, Canada
[4]Department of Highways, Bangkok, Thailand
[*]now at: Stockholm Univ., Dept. of Applied Environmental Science, Stockholm, SE, Sweden

Received: 20 April 2012 – Accepted: 24 April 2012 – Published: 8 May 2012

Correspondence to: P. J. Adams (petera@andrew.cmu.edu)

Published by Copernicus Publications on behalf of the European Geosciences Union.







## Abstract

Aerosol nucleation occurs frequently in the atmosphere and is an important source of particle number. Observations suggest that nucleated particles are capable of growing to sufficiently large sizes that they act as cloud condensation nuclei (CCN), but some global models have reported that CCN concentrations are only modestly sensitive to large changes in nucleation rates. Here we present a novel approach for using long-term size distribution observations to evaluate the contribution of nucleation and growth to the tropospheric CCN budget. We derive from observations at five locations nucleation-relevant metrics such as nucleation rate of particles at diameter of 3 nm ($J_3$), diameter growth rate (GR), particle survival probability (SP), condensation and coagulation sinks, and CCN formation rate. These quantities are also derived for a global microphysical model and compared to the observations on a daily basis to evaluate the model's CCN budget. Using the GEOS-Chem-TOMAS global aerosol model we simulate nucleation events predicted by ternary (with a $10^{-5}$ tuning factor) or activation nucleation over one year and find that the model does not understate the contribution of boundary layer nucleation to CCN concentrations. Model-predicted annual-average formation rates of 50 nm and 100 nm particles due to nucleation are always within 50 % and show a slight tendency to over-estimate the observations. Because it is rare for observations to track the growth of a nucleation mode across several days, it is difficult to assess CCN formation when growth requires multiple days. To address multi-day growth, we present three cases of survival of particles beyond one day: single-day growth, partial multi-day survival, and total multi-day survival. For the single-day growth case, only particles that reach a CCN size (50 or 100 nm) on the same day are counted as contributing to the CCN budget, which represents a low estimate of CCN attributable to nucleation. The partial survival case extrapolates the coagulation sink and growth rate allowing nucleated particles as much time as needed to become CCN and represents a realistic, but perhaps somewhat high, estimate for CCN formation from nucleation. The total survival case assumes that all particles that survive the





ACPD

12, 11765–11822, 2012



first day, no matter their end-of-day size, will eventually become CCN and represents a high estimate of CCN formation from nucleation. On days that the growing nucleation mode reaches 100 nm, median single-day survival probabilities to 100 nm for the model and measurements range from less than 1 % to 9 % across the five locations we considered. At the upper end, total survival median survival probabilities to 100 nm are no greater than 36 % and the partial survival case survival probabilities are 5 to 25 %, depending on the site. Using growth rates, nucleation rates, coagulation rates, survival probabilities, and an assumed CCN lifetime, we calculate that annually averaged CN100 concentrations (a proxy for CCN) formed from single-day nucleation and growth events does not exceed 50 $cm^{-3}$ in both the model and the measurements across the five locations, representing no more than 3 % of total CN100. When we extrapolate growth and loss to include growth to CCN beyond the first day (partial survival case), we find that both the model and measurements show a higher but still modest contribution (up to 14 %) to total CN100. This detailed exploration of new particle formation and growth dynamics adds support to the use of global models as tools for assessing the contribution of microphysical processes such as nucleation to the total number and CCN budget.

## 1 Introduction

Atmospheric aerosols are known to perturb climate in several ways. The largest current uncertainty in aerosol climate forcing is the aerosol indirect effect (AIE), which is broken down into the cloud albedo effect and the lifetime effect (Twomey, 1977; Albrecht, 1989). With increasing aerosols, a subset of which act as cloud condensation nuclei (CCN), brighter and potentially longer-lived clouds are formed. In order for aerosols to exert these influences on clouds, they are either introduced into the atmosphere by direct emission or gas-to-particle conversion (nucleation) where they may grow to sufficiently large sizes to act as CCN (Kerminen et al., 2005; Pierce and Adams, 2007; Kuang et al., 2009). A competition between condensational growth and coagulational





ACPD
12, 11765–11822, 2012



loss determines a particle's survival probability during growth through a certain size range (Fig. 1). Although subject to the same dynamic processes, the fates of particles formed via primary emission and nucleation can be quite different. Stable clusters of nucleating sulfuric acid vapor are typically 1 nm in size, which is much smaller than typical primary emission size ranges (Kulmala et al., 2000, 2004; Mäkelä et al.,1997; Vehkamaki et al., 2004). As a result, in order for particles formed via nucleation to act as CCN, they must grow via condensation while avoiding loss by coagulation for a longer amount of time and through a larger range of sizes than primary emissions. Since freshly nucleated particles are small, they are highly diffusive and prone to collide with pre-existing particles. Therefore, coagulation is very efficient between fresh nuclei and larger particles, compounding the difficulty that nucleated particles have in growing to CCN sizes. Ambient measurements presented in Kuang et al. (2009) highlight the importance of coagulation as at least 80 % of the nucleated particles on average are lost by coagulation before becoming CCN in the cases that they studied, even during days with high growth rates.

Recent work has suggested there is a potential discrepancy between aerosol models and observations regarding the number of CCN formed from nucleated particles. For example, the aforementioned. Kuang et al. (2009) study reported survival probabilities up to 20 % for measured nucleation events in Atlanta, GA and suggested inaccuracies in model-predicted organic condensation growth rates as a possible explanation for the difference with the model results of Pierce and Adams (2009b). Pierce and Adams (2009b) showed low probabilities (10 % or less) of particles growing to CCN sizes when nucleation parameterizations were active in the simulations. Using a global aerosol model, they also found that global CCN concentrations are more responsive to uncertainties in primary emissions than uncertainties in nucleation, reporting a 12 % global average CCN sensitivity when varying the nucleation rate by six orders of magnitude. Moreover, the low sensitivity was attributed to lower survival probabilities at higher nucleation rates. In the extreme case of fast ternary nucleation rates of Napari et al. (2002), particle survival probabilities were on the order of $10^{-8}$.





ACPD
12, 11765–11822, 2012



The differing outcomes between models and measurements as well as between different models are likely caused by several factors. First, models including the one employed in Pierce and Adams (2009b) may suffer from the lack of a robust nucleation theory. As will be explained, observed nucleation events cannot fully be explained by theory. Secondly, observational studies are often limited to a single location and a short length of time, and may focus on dramatic growth events that are not necessarily representative of the longer climatology. Third, models may also be inaccurate in secondary organic aerosol (SOA) formation, which is essential for the growth of nucleated particles to CCN sizes. The most recent estimates of the SOA budget have constrained it to fall within 50 to 230 $Tg\,SOA\,yr^{-1}$, although other studies have reported ranges as low as 12–70 $Tg\,SOA\,yr^{-1}$ (Kanakidou et al., 2005; Spracklen et al., 2011). Fourth, the endpoints of comparison between measurements and models are often not the same, making a side-by-side comparison erroneous or difficult. This is especially true in model-model comparisons of the contribution of nucleation to CCN, in which the problem is rooted in the difference between the fractional contribution of nucleation to CCN and the sensitivity of CCN to changes in nucleation.

The science behind nucleation theory is not well understood and many plausible yet not fully robust formulations have been proposed. The importance of sulfuric acid as a primary nucleating species has been confirmed (Berndt et al., 2005; Kuang et al., 2008; Sipilä et al., 2010; Vuollekoski et al., 2010; Weber et al., 1996). Additional evidence has shown that low volatility organic vapors (Paasonen et al., 2010; Zhang et al., 2004), amines (Bzdek et al., 2010; Kurtén et al., 2008; Kirkby et al., 2011), and ammonia (Ball et al., 1999; Erupe et al., 2010; Kirkby et al., 2011) may also play significant roles in the initial steps of atmospheric nucleation. Binary and ternary homogenous nucleation theories have been proposed to explain nucleation rates on a global scale in the atmosphere. Binary homogenous nucleation involves the supersaturation of solutions of sulfuric acid and water in a binary system (Vehkamaki et al., 2004). Ternary homogenous nucleation, such as the parameterization proposed by Napari et al. (2002), adds a third nucleating species, typically ammonia ($NH_3$). The original





ACPD
12, 11765–11822, 2012



ternary formulation of Napari et al. (2002) showed high biases in predictions of nucleation rates and aerosol number concentrations (Merikanto et al., 2007). A modified version with a globally constant nucleation rate tuning factor of $10^{-5}$ has been incorporated into a regional aerosol model and shows much better agreement (Jung et al., 2010) with observations. Other possible nucleation parameterizations include empirical methods such as activation nucleation (Kulmala et al., 2000), which is often applied in the planetary boundary layer (PBL) in conjunction with the binary scheme of Vehkamaki et al. (2004) in the free troposphere.

Adding to the poor understanding of atmospheric nucleation is the role of charged particles. Recently, Yu and Turco (2011) reviewed previous findings and suggested a 100 % contribution of ions to new particle formation at Hyytiälä. However, other studies have found no greater than a 10 % contribution of ion nucleation to aerosol formation rates in similar continental boundary layer environments (Gagné et al., 2008, 2010; Laakso et al., 2007; Manninen et al., 2009). Kirkby et al. (2011) showed that ion-induced binary nucleation is not likely to play a role in boundary layer nucleation but may be important for the free troposphere at temperatures around 250 K. Kazil et al. (2010) suggested that ions may play an important role in nucleation in the marine boundary layer; however, to our knowledge this has not been explored yet by observations.

Freshly formed nuclei have very short lifetimes in the atmosphere (less than a few hours for 1–5 nm particles in the boundary layer) due to loss by coagulation with larger particles. Thus, they must grow quickly to larger sizes if they are to influence CCN concentrations. Once nuclei are formed, growth is typically dominated by condensation of sulfuric acid vapor and low volatility organic vapors. At some locations, organic condensation accounts for nearly the entire aerosol diameter growth rate (Kuang et al., 2009; Riipinen et al., 2011). Diameter growth rates from 3 to 25 nm during nucleation events in 2007 at Hyytiälä, Finland have a median value of 2.3 $\mathrm{nm\,h^{-1}}$, although median rates up to 8.9 $\mathrm{nm\,h^{-1}}$ have been reported for a continental location in South Africa (Vakkari et al., 2011). Coagulational growth of nucleated particles can also occur





ACPD
12, 11765–11822, 2012



when similar sized small nuclei interact with each other, although this self-coagulation is much smaller than condensation growth and can generally be ignored (Dal Maso et al., 2002; Kerminen and Kulmala, 2002; Stolzenburg et al., 2005). More commonly, coagulation scavenging occurs, which is the dominant sink of freshly formed nuclei compared to deposition, but is highly dependent on atmospheric conditions (Pierce and Adams, 2007). Understanding the growth and loss processes, which make up a particle's survival probability, is the most important step in understanding the contribution of nucleation events to aerosol number and CCN concentrations.

To date, modeling studies aiming to quantify CCN formation from nucleation have been limited by a lack of detailed evaluation of modeling output against ambient observations and have suffered from the nonlinear nature of aerosol microphysics when making sensitivity calculations. Because of feedbacks on condensation and coagulation, the common methodology of "turning off" nucleation as a control experiment against a nucleation-active simulation is useful for sensitivity calculations but is not equal to a fractional contribution of nucleation to CCN. Studies have reported CCN sensitivities to nucleation ranging from 3–60 % (Yu and Luo, 2009; Makkonen et al., 2009; Merikanto et al., 2009; Spracklen et al., 2010; Wang and Penner, 2009). Each of these studies used different models and often significantly different inputs, assumptions, and metrics for assessing CCN sensitivity, making model intercomparison difficult. In particular, the domain over which nucleation is changed (boundary layer or free troposphere), CCN activation scheme, and the definition of what counts as a "nucleated" particle can influence results significantly. For example, Pierce and Adams (2009b) chose binary and ternary nucleation as the two endpoints for a sensitivity study, whereas others such as Spracklen et al. (2008) turn nucleation off entirely in a global model as a control against simulations with any particular active nucleation theory. Spracklen et al. (2008) found the influence of nucleation on CCN (0.2 %) to be as low as 3 % and as large as 20 %. However, these values refer only to the sensitivity of CCN to activation nucleation in the boundary layer. Merikanto et al. (2009) found that 45 % of CCN (0.2 %) originate from nucleation, although they note that most of that (35 % of CCN) comes





ACPD
12, 11765–11822, 2012



from the free and upper troposphere and not the boundary layer. Yu and Luo (2009), who found the highest contribution to CCN of all of the studies, assumed that 5 % of the sulfate formed in plumes on sub-grid spatial scales (e.g., Stevens et al., 2012) exists in the nucleation mode and counts towards the nucleation contribution to CCN. Other cited studies include only regional-scale (i.e. grid-scale resolved) nucleation events in the nucleation contribution. Additionally, the aerosol microphysics model employed in Yu and Luo (2009) used a fixed lognormal mode to prescribe primary organic aerosol size, resulting in a simplified treatment of the coagulation of nucleation particles with larger, primary particles. Makkonen et al. (2009) use the ECHAM5-HAM cloud droplet activation scheme and report CCN enhancements of up to 50 % in the boundary layer between activation and binary nucleation. The ECHAM5-HAM cloud droplet activation scheme allows nucleated particles to become CCN active as soon as they grow to 35 nm wet radius and treats all particles larger than 35 nm wet radius as equal for purposes of activation. This translates to roughly a 50 nm dry activation diameter, a value that may tend to overstate the impact of nucleation on CCN formation. Finally, Wang and Penner (2009) use the IMPACT aerosol model incorporated into the NCAR CCSM3 to determine a 5.3 % enhancement in CCN due to nucleation.

The Makkonen et al. (2009) study and the Yu and Luo (2009) study show the highest CCN sensitivity to nucleation but also use very different assumptions in terms of activation scheme and what counts as nucleation. The works of Spracklen et al. (2010), Spracklen et al. (2008), and Merikanto et al. (2009) find free troposphere nucleation to be a major source of their nucleated particles growing to CCN, something that the Pierce and Adams (2009) study does not explicitly test. Bearing in mind the differences in the reported calculations, the 3–60 % range in CCN sensitivity to nucleation is likely more apparent than real. Although the diversity of simulations is useful, we suspect that models would agree more closely with each other when using a consistent basis of comparison. In particular, omitting the Makkonen et al. (2009) and Yu and Luo (2009) studies, the range of influence of boundary layer nucleation on CCN is much narrower.





ACPD
12, 11765–11822, 2012



Therefore, it is necessary to perform detailed comparisons between models and observations to assess whether models are indeed biased or whether discrepancies are more apparent than real. Quantifying survival probability and CCN formation efficacy can be done with both ambient data and modeling output. Here we build upon previous studies to show how size distribution observations can be used to infer CCN formation rates from nucleation on a long-term (one year) basis. The result is an observational constraint on the contribution of nucelation to the overall CCN budget. In this paper, we analyze ambient measurements and model output and calculate relevant nucleation metrics such as the nucleation rate, growth rate, condensation and coagulation sink, survival probably, and CCN formation. We present an evaluation of model results by comparing to the nucleation metrics calculated for ambient measurements. We recommend that future modeling studies of nucleation and CCN use these similar metrics to allow for straightforward comparisons between models and with observations. Uncertainties in nucleation theories and growth mechanisms dictate that global aerosol microphysics models must be evaluated against nucleation-relevant observations in order to be used in a predictive capacity. We first perform a detailed evaluation of nucleation dynamics with ambient measurements at five locations and then determine the contribution of nucleation to CCN in both the ambient observations and a global aerosol microphysics model, GEOS-Chem-TOMAS.

## 2 Models and analysis

### 2.1 GEOS-Chem

The Goddard Earth Observing System global chemical transport model (GEOS-Chem) version 8.3.1 is used for this study (Bey et al., 2001; http://geos-chem.org/). The version of GEOS meteorological fields used was either GEOS-3 or GEOS-5, as required by the simulation period (Table 1). In all simulations, 4° by 5° latitude by longitude resolution is used with either 30 or 47 vertical sigma-coordinate layers extending from the surface





ACPD
12, 11765–11822, 2012



to 0.01 hPa. GEOS-Chem v8.3.1 contains all of the features described in Trivitayanurak et al. (2008) with the following updates. Anthropogenic emissions are treated with the Emissions Database for Global Atmospheric Research (EDGAR) inventory but are often overwritten by a number of regional inventories (Olivier et al., 1996). These regional inventories include Big Bend Regional Aerosol and Visibility Observational Study (BRAVO) emissions inventory for Mexico and Southwestern US, Criteria Air Contaminants (CAC) for anthropogenic emissions over Canada (http://www.ec.gc.ca/inrp-npri/), the Cooperative Programme for Monitoring and Evaluation of the Long-range Transmission of Air Pollutants in Europe (EMEP), EPA National Emissions Inventory (NEI) for the United States (http://www.epa.gov/oar/data/neidb.html), and the Streets inventory for Asian emissions (Kuhns et al., 2003; Auvray and Bey, 2005; Bond et al., 2003). Biogenic emissions in the model follow the MEGAN database, and biomass burning emissions use the Global Fire Emissions Database version 2 (GFEDv2) (Randerson et al., 2006; Guenther et al., 2006). $NO_x$ emissions from aircraft, lightning, and soil are considered in the global model. Shipping $SO_x$ emissions are considered within EDGAR and EMEP.

## 2.2 TwO-Moment Aerosol Sectional (TOMAS) algorithm

Aerosol microphysics calculations are performed with the TwO Moment Aerosol Sectional algorithm (TOMAS), which is hosted by the GEOS-Chem global chemical transport model. Generally, we employ the work of Trivitayanurk et al. (2008) with the organic aerosol additions of Pierce et al. (2007), the dust additions of Lee et al. (2009), and the nucleation implementations of Pierce and Adams (2009a). TOMAS was introduced as a standard component of GEOS-Chem in version 8.3.1 and is available for download (http://www.geos-chem.org). TOMAS is a modular algorithm that contains codes to calculate the effects of nucleation, coagulation, condensation/evaporation, cloud processing, size-resolved dry and wet deposition, and emissions on the number and mass size distribution of aerosols (Adams and Seinfeld, 2002; Tzivion et al., 1987). The aerosols are split up into 9 chemical species including sulfate, sea salt, hydrophilic and





ACPD
12, 11765–11822, 2012



hydrophobic organic carbon, externally and internally mixed elemental carbon, mineral dust, ammonium, and aerosol water. Each component is tracked across 40 logarithmically spaced size sections or "bins" with a range of 1.1 nm to 10 µm. Size-resolved deposition, coagulation, condensation, and cloud processing are unchanged from Trivitayanurak et al. (2008). Primary sulfate aerosol emissions are 1 % of anthropogenic $SO_2$ emissions and use the size distributions described in Adams and Seinfeld (2003). Sea salt emissions are treated in the same manner as in Trivitayanurak et al. (2008). Organic aerosols were not included in Trivitayanurak et al. (2008) but are included in the present work and described in the next section. Advection, chemistry, and deposition have remained largely unchanged from the work of Trivitayanurak et al. (2008), although periodic minor updates in both advection and chemistry (e.g. newer reaction rate constants and photolysis constants) have been implemented into successive versions of GEOS-Chem.

Activation to cloud condensation nuclei is based on Köhler theory (Raymond and Pandis, 2003), which is incorporated via look-up tables that take percent composition of sulfate, sea salt, organic carbon and insoluble material as inputs and yield critical activation diameters at various supersaturations as output. Below we highlight some recent additions to GEOS-Chem-TOMAS.

### 2.2.1 Organic aerosol

Carbonaceous aerosols are configured in a similar manner to Pierce et al. (2007). Organic aerosol is divided into four sub-categories: externally mixed EC, internally mixed EC, hydrophobic OC, and hydrophilic OC. The contributions of each of the organic categories to CCN activity is represented using the single, lumped, hygroscopicity parameter ($\kappa$) of Petters and Kreidenweis (2007). We assume a constant OM : OC ratio of 1.8 for all emissions and for ambient organic aerosol (El-Zanan et al., 2005; Zhang et al., 2005). The effect of organic aerosol on surface tension depression (Facchini et al., 1999; Nenes et al., 2002) in activating cloud drops is not considered. The timescale





ACPD
12, 11765–11822, 2012



of conversion of hydrophobic to hydrophilic aerosol was 1.5 days. Conversion from externally mixed to internally mixed EC uses this same timescale.

Secondary organic aerosol (SOA) is considered to be entirely non-volatile and does not react or partition between the aerosol and gas phase. Instead, SOA in TOMAS is calculated as 10 % of global monoterpene emissions, resulting in approximately 19 Tg yr$^{-1}$ of SOA. The SOA condenses to all particles based on their Fuchs surface area (Pandis et al., 1991). Although there is overwhelming evidence for the thermodynamic partitioning of semi-volatile organic aerosols (Donahue et al., 2006), the non-volatile, kinetic condensation SOA treatment used here is simple and performed well in earlier nucleation studies that compared to observed aerosol number concentrations and growth rates (Riipinen et al., 2010; Pierce et al., 2011).

### 2.2.2 Nucleation

Several changes have been made to the treatment of nucleation in GEOS-Chem-TOMAS since Trivitayanurak et al. (2008). Sulfuric acid is now calculated using a pseudo-steady state approach for each time step (Pierce and Adams, 2009a). Nucleation is treated using either ternary nucleation (Napari et al., 2002) with a $10^{-5}$ tuning factor or activation nucleation (Sihto et al., 2006) with an $A$ factor of $2 \times 10^{-6}$ ($s^{-1}$). We have chosen an $A$ in the range found to be most atmospherically applicable based on measurements in the continental boundary layer (Sihto et al., 2006; Riipinen et al., 2007), however results are somewhat sensitive to the $A$ factor choice within reasonable bounds (Spracklen et al., 2009). The size resolution down to 1.1 nm allows for explicit simulation of the dynamics of fresh nuclei. The model saves size distributions at 30-min time steps at each of the five locations for comparison against highly time resolved ambient measurements.





ACPD
12, 11765–11822, 2012



## 2.3 Ambient measurements

Table 1 outlines the five locations where we have obtained size distribution data; Pittsburgh, Hyytiälä, Atlanta, St. Louis, and San Pietro Capofiume (also referred to as Po Valley from this point forward). These locations span a range of conditions, making the set a good test for a global aerosol microphysics model. For instance, growth at Hyytiälä is dominated by organic condensation, whereas at Pittsburgh, sulfuric acid condensation is the leading mechanism for particle growth. All of the sites except for Hyytiälä are polluted sites, and all of those except for Po Valley are urban polluted locations. At each of the sites, size distribution measurements were made for at least one continuous year with either a Scanning Mobility Particle Sizer (SMPS) or Differential Mobility Particle Sizer (DMPS). Sulfuric acid measurements were made at Hyytiälä using a Chemical Ionization Mass Spectrometer (CIMS) (Petäjä et al., 2008). Time resolution in the size distribution observations was typically a little finer than in the model output as all sites recorded measurements in no longer than 15-min intervals. Analysis of both the ambient measurements and model output used the same procedure for calculating nucleation relevant quantities (e.g. growth rates and survival probabilities) from size distribution data (see Sect. 2.5).

## 2.4 Simulations

Simulations were performed over a time period coinciding with the times that the observations were taken. This ability to perform near real time simulations is a strength of the assimilated meteorology employed by GEOS-Chem. Each of the years of comparison are listed in Table 1. For Hyytiälä, the year of comparison used is 2007. The Pittsburgh, Po Valley, Atlanta, and St. Louis measurement periods were all several years earlier ranging from 1999 to 2003. For each location, two simulations were performed reflecting the two nucleation schemes tested: ternary nucleation (Napari et al., 2002) with a $10^{-5}$ tuning factor and activation nucleation (Sihto et al., 2006) in the boundary layer coupled with binary nucleation (Vehkamaki et al., 2004) elsewhere. Thus, in total we





ACPD
12, 11765–11822, 2012



ran 10 simulations for 14 months, which accounts for 2 months of model spinup. For each model grid cell corresponding to the location of the measurements, number size distribution and sulfuric acid concentration output was saved for analysis and comparison with measurements.

### 2.5 Nuclei fate analysis and CCN formation potential

To calculate nucleation rates and infer the fates of nucleated particles, we have modified a series of nucleation dynamics codes for Hyytiälä data referenced in Dal Maso et al. (2005). These codes, which have been modified slightly for use with TOMAS output and other ambient datasets, calculate formation rates of 3 nm particles, diameter growth rates, condensational and coagulational sinks, absolute number concentration, particle survival probability, formation rates of 50 and 100 nm particles, and steady-state cloud condensation nuclei concentrations attributable to nucleation and growth events. The following sections outline the method of calculation for each of these metrics.

#### 2.5.1 Frequency of events

For nucleation event frequency, our methods are similar to those outlined in Dal Maso et al. (2005). The evolution of the particle size distribution over the course of the day ("banana plot", Fig. 2) reveals some features that we use to identify nucleation events. First, a distinctly new nucleation mode (1–25 nm) of particles must appear in the size distribution. Secondly, the new mode must last at least 2 h and show signs of growth. Figure 2 shows example measured and modeled nucleation events. For example, at about 14:00 UTC at Pittsburgh, PA, on 16 April, 2002, a large number of 3 nm particles were measured to appear and subsequently grow as evidenced by the red contours (black dashed line) moving up in both diameter space and time.





ACPD
12, 11765–11822, 2012



### 2.5.2 Formation rate and growth rate

Formation rate (or nucleation rate) of 3 nm particles ($J_3$) is calculated from the time derivative of nucleation mode number concentration ($N_{3-25}$) with a coagulation correction ($F_{coag}$) representing scavenging of small particles by pre-existing aerosol (Eq. 1). Note that the flux of particles out of the size range ($F_{growth}$) term is not included here. This term is neglected because particles do not often grow beyond 25 nm while the nucleation burst is still occuring (Dal Maso et al., 2005). The values of $J_3$ are averaged over 24-h periods for consistency in comparisons (more details in Sect. 2.5.4). Therefore, all else being equal, a longer nucleation event will result in a higher $J_3$ value for that day compared to a shorter event. This facilitates subsequent analysis of the particle number budget and avoids the need for a semi-arbitrary determination of precisely when the nucleation event began and ended.

$$J_3 = \frac{dN_{3-25}}{dt} + F_{coag} \quad (1)$$

The size distribution function is integrated over the 3–25 nm size range to get the absolute number concentrations, which vary with time. The coagulation correction is the product of the 3–25 nm number concentration and the corresponding coagulation sink (described in Sect. 2.5.3) for a particular larger size, integrated across all particles larger than 25 nm. Zhang et al. (2010a) and Zhang et al. (2010b) compared observed nucleation rates at Atlanta to various model parameterizations in a similar manner as we have summarized here.

Diameter growth rates (GR) are calculated by considering the peak of the size distribution at 3 nm and 25 nm. We fit a first-order polynomial to the maximum value of the size distribution as it varies over time. The slope of the fitted line is the diameter growth rate. An additional growth rate is calculated for the 25 to 100 nm size range for purposes of the condensational growth timescale calculation, explained in Sect. 2.5.3. Since the growth rate does not vary much within the nucleation or Aitken mode for the modeled and measured nucleation events, this assumption is justified.





ACPD
12, 11765–11822, 2012



### 2.5.3 Coagulation and condensation sinks

Calculation of coagulational and condensational growth is adapted from the Probability of Ultrafine Growth (PUG) model, introduced by Pierce and Adams (2007). Loss of small nuclei by collisions with larger, pre-existing aerosol is the major pathway preventing growth of nucleated particles to Aitken mode and larger sizes. The frequency of coagulational loss, CoagS ($s^{-1}$), of particles of size $i$ to a larger size $j$ is dependent on a coagulation coefficient ($K_{ij}$) and the number concentration in the larger size range, $N_j$ (Eq. 2). Coagulation of particles of the same size is represented by the first term in Eq. (2). The CoagS term is both size and time dependent. In our calculations, we set the initial size to either 1 or 3 nm (the lower size cutoff of the model and measurements, respectively) and calculate coagulation coefficients for all particles larger than size $i$. The coagulation coefficient is based on Fuchs equation (Seinfeld and Pandis, 2006).

$$\mathrm{CoagS}_i = \frac{1}{2}K_{ii}N_i + \sum_{j=i+1}^{\max} K_{ij}N_j \tag{2}$$

The condensation sink describes the first-order rate of uptake of sulfuric acid or other condensable vapors to aerosols (Eq. 3). In the kinetic regime, the condensation sink is proportional to surface area and is proportional to particle diameter in the continuum regime.

$$\mathrm{CS} = 2\pi D \sum_{i=1}^{\max} \beta_i D_{pi} N_i \tag{3}$$

In Eq. (3), the condensation sink (CS) is calculated from the gas-phase diffusion constant ($D$), particle diameter in size bin $i$ ($D_{pi}$), number concentration in size $i$ ($N_i$), and the transition regime (connecting the kinetic and continuum regimes) correction factor $\beta_i$, which is dependent on the Knudsen number (Seinfeld and Pandis, 2006). The condensational growth timescale, not to be confused with condensation sink, is the time





ACPD
12, 11765–11822, 2012



it takes for a particle to grow to a size of interest. The coagulation timescale is the inverse of the coagulation sink for a given size range. These two timescales (Eqs. 4 and 5) are required for the survival probability calculation (Sect. 2.5.4). In physical terms, the timescales represent the amount of time it takes for particles in size range $k$ to grow or be lost to larger sizes.

$$\tau_{k,k+1}^{\text{cond}} = \frac{D_{p,k+1} - D_{p,k}}{\text{GR}_{k,k+1}} \tag{4}$$

$$\tau_{k}^{\text{coag}} = \frac{1}{\frac{1}{2}\text{K}(D_{p,k}, D_{p,k})N_k + \sum_{j=k+1}^{k_{\max}} K(D_{p,k}, D_{p,j})N_j} \tag{5}$$

In Eq. (5), similar to Eq. (2), the first term in the denominator represents self-coagulation of particles in the same size bin. The second term represents coagulation with particles in larger size bins, up to the model or measurement maximum size, $k_{\max}$.

### 2.5.4 Survival probability and CCN formation

We define survival probability as the ratio of particle fluxes at the initiation point of growth (typically $J_3$) and the CCN-relevant size or endpoint of growth ($J_n$, with $n = 50$ or 100 nm typically). Figure 1 highlights the sources and sinks of particles throughout nuclei growth. Within our analysis, survival probability (SP) is calculated using two intermediate calculations of coagulational loss and condensational growth timescales. Both timescales (Eqs. 4 and 5), are calculated for nucleation mode as it grows with time. Similar to Kuang et al. (2009), we calculated a single survival probability for each nucleation event corresponding to the trajectory of particles following the maximum value of the nucleation mode (dashed line in Fig. 2). Thus, for each timestep (30 min for the model, shorter for measurements) the instantaneous coagulational loss and condensational growth timescales are calculated. The overall survival probability, shown in Eq. (6), from size $m$ to $n$ (here, 3 to 100 nm or 3 to 50 nm), is calculated as the product





ACPD
12, 11765–11822, 2012



of individual probabilities across smaller size ranges, represented by the exponential term inside of the product in Eq. (6). In physical terms, this method calculates the probability of nuclei growth from one discrete size (or section for model output) to the next largest size. Taking the product of these individual probabilities yields a survival probability from fresh nuclei to CCN-relevant sizes.

$$\mathrm{SP}_{m,n} = \prod_{k=m}^{n-1} \exp\left(-\frac{\tau_{k,k+1}^{\mathrm{cond}}}{\tau_k^{\mathrm{coag}}}\right) \quad (6)$$

The formation rate of 100 nm particles ($J_{100}$) is calculated as the 3 nm formation rate multiplied by the survival probability from 3 to 100 nm (Eq. 7). Likewise, $J_{50}$ is calculated as $J_3$ multiplied by the survival probability to 50 nm. These two particle sizes are within the range of typical activation diameters for CCN concentrations. Although this method does not consider particle composition, under typical supersaturations, many particles of 50 or 100 nm in size will activate to CCN. For atmospheric conditions most typical for the indirect effect, stratiform clouds and mixed inorganic-organic particles, the 100 nm size is probably the most appropriate CCN surrogate. However, because few nucleation and growth events reach the 100 nm cutoff ($n = 100$ in Eq. 7) on the same day, an analysis focusing on the 100 nm cutoff necessarily excludes a large number of useful observations. Therefore, we also compare survival results for 50 nm ($n = 50$) between model and observations, which is still CCN relevant and includes a larger number of events (see later discussion of Table 5).

$$J_n = \mathrm{SP}_{3-n} J_3 \quad (7)$$

Using the CCN formation rate as well as estimates of CCN lifetime we obtain annually averaged CCN ($\mathrm{CN50_{nuc}}$ and $\mathrm{CN100_{nuc}}$) concentrations attributable to single-day nucleation and growth events according to Eq. (8). Note that Eq. (8) is written for $\mathrm{CN100_{nuc}}$ but the same basic equation applies for $\mathrm{CN50_{nuc}}$ with the substitution of





ACPD
12, 11765–11822, 2012



$SP_{3–50}$:

$$CN100_{nuc} = \frac{1}{365\ \text{days}} \left[ \sum_{\text{days}} (J_3)\,(SP_{3–100})\,(24\,\text{h}) \right] \tau_{CCN} \quad (8)$$

Note that the $J_3$ values used in this equation are already daily averaged (see Sect. 2.5.2), so Eq. (8) already accounts implicitly for the varying length of the nucleation events. To convert CCN formation rates to CCN concentrations, a CCN lifetime ($\tau_{CCN}$) of 7 days is assumed.

Because of a lack of reliable multi-day measurements, it is difficult to assess the survival probabilities and CCN formation potential for nucleated particles beyond the first day of observations. In attempt to address this shortcoming, we extend our CCN and survival analysis in a couple of ways. First, we recognize that the single-day analysis, which gives nuclei only 24 h to grow to CCN sizes, is a lower bound estimate on CCN. We refer to this as the "single-day" case (Table 6). Next, we add an upper estimate by allowing any particles that survive the first day to act as CCN (either $CN50_{nuc}$ or $CN100_{nuc}$) without coagulating. Since this upper estimate, referred to as the "total survival" case, assumes perfect survival probability on all days after the first, it cannot be considered very plausible. Last, we add an extrapolation estimate ("partial survival"), which falls in between the upper and lower bounds. This estimate extrapolates the 25–100 nm growth rate and coagulational loss rates at the end of the growth period and applies it to subsequent days, allowing particles to either grow to CCN sizes or be lost via coagulation at a later time. We judge that the partial survival estimate probably overstates the ultimate CCN formation for several reasons. First, while real nuclei do not grow overnight but are lost to coagulation, we extrapolate the daytime growth rate for all subsequent hours. Second, it is expected that growth rates on nucleation days are somewhat higher than average. Third, it is expected that the coagulation sink on nucleation days is somewhat lower than average (Gong et al., 2010; Wu et al., 2011). Whereas our single-day analyses are most useful for direct model-measurement comparison since they require no assumptions regarding the fate of particles beyond that





ACPD
12, 11765–11822, 2012



day, we add these two extra estimates to provide a stronger basis for evaluating the eventual impact of nucleation on CCN. Results using these estimates are discussed in Sect. 3.4.

## 3 Results

Figure 2 shows sample boundary layer nucleation events in the ternary nucleation model and in the ambient observations. At Pittsburgh on 16 April, strong growth to 80 nm is seen in the observations and in the ternary model. Figures 3 and 4 show results for new particle formation event frequency, both on a yearly and monthly basis. Figures 5–9 are cumulative distribution functions of nucleation and growth metrics from the year of simulations and observations separated by each site. The quantities chosen for model-measurement comparison are formation rate ($J_3$), growth rate (GR), survival probability ($SP_{50}$ and $SP_{100}$), and 50 and 100 nm particle formation rates ($J_{50}$ and $J_{100}$). Each point in the CDF of a given nucleation metric represents one nucleation event (or one day) for that specific metric. These plots include only data and model output from the subset of days that are categorized as nucleation events according to the methodology described in Sect. 2.5.1. For the CCN formation rate and survival probability panels of the CDF figures, days where the nucleation mode does not grow to the particular cutoff size (50 or 100 nm) are not included in the figure. The number of these days for each site in the model and the observations can be seen in Table 5. The formation rates are averaged over 24 h, as is explained in Sect. 2.5.4. Figures 10 and 11 add a few more metrics such as condensation sink, sulfuric acid concentrations, and speciated growth rates. Figure 12 shows the resulting single- and multi-day nucleation event contribution to annually averaged $CN50_{nuc}$ and $CN100_{nuc}$ at each of the five cities.





ACPD
12, 11765–11822, 2012



### 3.1 Overview of model-measurement comparison results by location

At each site, event frequency (Fig. 3) is predicted well by both the ternary and activation model cases. The bars represent number of events and the percentages over the bars represent the number of specific days that are correctly modelled as either events or non-events. Among the five cities, the scaled ternary simulation overpredicts the number of events over the year by as few as 5 days and as many as 31 days. The activation simulation tends to overpredict somewhat more than the ternary simulation (20 to 64 days across the five cities). As seen in Fig. 3, there were 109 observed nucleation events during the campaign time domain in Pittsburgh and TOMAS predicts 114 and 129 for the ternary and activation cases, respectively. The model does best at Pittsburgh and Hyytiälä, where 60–70 % of the exact days are correctly modelled as either events or non-events. For the metrics compared in Fig. 3, the model consistently shows somewhat more accurate predictions with ternary nucleation when compared to activation.

Figure 4 shows the seasonal breakdown of events on a month by month basis. In general, the model shows mixed performance in following the seasonal trend, except at Hyytiälä, where the seasonal trend is almost perfectly reproduced by the model ($R$ = 0.8). The model performs better here than any other site, which may be because the activation nucleation parameterization was developed with data from Hyytiälä. Additionally, spatial homogeneity and the lack of strong local sources at Hyytiälä also probably play a role. For models with coarse spatial resolution, spatially homogenous sites such as Hyytiälä make for ideal comparisons. Another possibility is the use of the more recent GEOS-5 meteorological fields at Hyytiälä, which were not used at any of the other sites. At Pittsburgh ($R$ = 0.23), events are overpredicted in the early winter months (January–March), but underpredicted in the fall months (September–November). Overprediction in the early winter months appears to be a common theme among other locations as well. The model does quite well in the spring and summer months, with near exact prediction in May at Pittsburgh (13 events observed, 11





ACPD
12, 11765–11822, 2012



predicted by ternary nucleation, 13 by activation coupled with binary). Results for June in Pittsburgh are missing because of instrument failure and data loss. St. Louis, Atlanta, and to some extent Po Valley show surprisingly similar behavior in the model; nucleation events are at maximum in the winter and minimum during the summer months. This behavior appears to be occurring at many locations within the model and is at least somewhat representative of observed seasonal trends at Atlanta and St. Louis, but not in the Po Valley ($R$ = 0.07). Although one might expect nucleation primarily in the summertime due to enhanced photochemical activity, colder temperatures favor nucleation in the wintertime (Dal Maso et al., 2005). At Hyytiälä and Pittsburgh, the strong nucleation in spring and fall may result from the balance between these two factors. Seasonal variations in prevailing wind direction, boundary layer height and cloudiness may also be important in some locations (Jaatinen et al., 2009). The observed seasonal cycle of nucleation is an important test of the models that requires further attention.

Figures 5–9 show the modelled and measured comparisons for each of the nucleation and growth metrics. Each figure contains comparisons for one year of nucleation events at a specific location: Pittsburgh, Hyytiälä, Atlanta, St. Louis, and Po Valley. Tables 2 and 3 show the median and mean values of each metric. Table 4 shows log-mean normalized biases (LMNB, the average number of orders-of-magnitude error) for modelled versus measured quantities.

As an example of the comparisons, Fig. 5 shows results for Pittsburgh. Overall, both the ternary and activation model agree well with observations at Pittsburgh (red trace in Fig. 5), as evidenced by the tight agreement in the empirical CDFs and the small bias values (Table 4). For example, the median growth rate of 2.4 $\mathrm{nm\,h^{-1}}$ at Pittsburgh is very accurately predicted by the ternary model (2.4 $\mathrm{nm\,h^{-1}}$) and activation (2.8 $\mathrm{nm\,h^{-1}}$). The accurate survival probability predictions at Pittsburgh (Fig. 5c, e) result from an overprediction the growth rate (Fig. 5b) and an underprediction in coagulation frequency. The modelled formation rates of CCN-sized particles (Fig. 5d, f) are generally in agreement with the measurements. However, some deviations exist, particularly with the activation and binary coupled nucleation simulation, which fails to predict the ~ 10 %





ACPD
12, 11765–11822, 2012



of nucleation events that result in strong formation rates ($> 0.1\,cm^{-3}\,s^{-1}$) of 100 nm particles (Fig. 5f).

Figures 6–9 show the comparisons of the same metrics at Hyytiälä, Atlanta, St. Louis, and the Po Valley. One particularly interesting result is the modelled and measured growth rates at Hyytiälä (Fig. 6b). Despite a relatively simple treatment of SOA in the global model, growth rates at the organic-dominated location are not underpredicted by TOMAS with either the ternary or activation nucleation schemes. Although we are on the lower end of expected global SOA formation ($19\,Tg\,yr^{-1}$), the completely non-volatile treatment of organics favors condensation onto the freshly nucleated particles (Riipinen et al., 2011). These inaccuracies may offset one another and result in modelled growth rates closer to observed. The growth rate in the model is driven mainly by organic condensation and not by sulfuric acid (Fig. 11). Additionally, the good model performance at Hyytiälä may be because it is a biogenic SOA dominated site, which is probably better represented in the global model when compared to anthropogenic SOA. Sect. 3.3 has additional comments on the speciated growth rate results, summarized for all of the five locations in Fig. 11.

In the comparisons for Atlanta in Fig. 7, we see worse model-measurement agreement than at Hyytiälä or Pittsburgh, particularly in the formation rates in Fig. 7a, d, f. Formation rates of 100 nm particles are overpredicted by up to a factor of 5 (LMNB $\sim 0.6$) and the discrepancy is similar for 3 and 50 nm formation (note the coarser axes in Fig. 7d). Figure 8 shows that comparisons at St. Louis are also worse than Hyytiälä or Pittsburgh for most metrics, especially the survival probability comparisons (Fig. 8c, e) which are generally overpredicted by the model by as much as a factor of 2. Finally, Fig. 9 (Po Valley) has some of the highest observed growth rates, and both nucleation assumptions in the model capture this quite well (Fig. 9b). Accordingly, this site is also on the high end of survival probability and 100 nm formation rate ($J_{100}$). This is consistent with Laaksonen et al. (2004), which found fast growth, high survival and high CCN formation at San Pietro Capofiume, Italy (Po Valley).





ACPD
12, 11765–11822, 2012



### 3.2 Sulfuric acid, condensation sink, and coagulation sink

Sulfuric acid measurements were available at Hyytiälä, and the comparison with model values is shown in Fig. 10. Only daily maximum sulfuric acid values are plotted here. Generally, sulfuric acid is overpredicted in the ternary model. The sulfuric acid concentrations in both the observations and the model are on the order of 1–$3 \times 10^6$ molecules cm$^{-3}$. Sulfuric acid in the activation model simulation is not plotted due to similarity (less than 20 % different) with the ternary model. Shown in Fig. 10b is the comparison between model and measured condensation sink. The modelled condensation sink is biased slightly low (LMNB $\sim -0.1$), which may reflect a weakness in the model's representation of pre-existing, background accumulation mode aerosol. However, this small bias does not seem to be strong enough to compromise many of our nucleation metric evaluations. Figure 10c is the CDF of coagulational sink of 3 nm particles. The ternary and activation/binary simulations show fair agreement with small negative bias, similar to the condensation sink comparisons in Fig. 10b.

### 3.3 Contributions of organics to modelled and measured particle growth

We also analyzed the relative contributions of sulfuric acid and low volatility organic vapors to the growth of nucleated particles in order to test whether the model underpredicts the SOA contribution to the growth rate. Figure 11 shows the annually averaged speciated growth rate for all sites. Sulfuric acid measurements were only available to us at Hyytiälä. As a result, only observations at Hyytiälä are broken down by organic or sulfuric acid growth. Total (nonspeciated) growth rate is instead plotted for the four other sites (yellow bars with green stripes in Fig. 11). The measurements at Hyytiälä and the model at some locations (Hyytiälä, St. Louis, Po Valley) show a strong organic component in what is condensing and causing particle growth. Sulfuric acid is not particularly an important component of the growth rate at Hyytiälä, but is more important for nucleation rates and frequency of events. This is consistent with findings in Riipinen et al. (2011). In contrast, Pittsburgh and Atlanta appear to be dominated by





ACPD
12, 11765–11822, 2012



sulfuric acid condensation in the model. This is realistic for Pittsburgh, a location heavily impacted by power plant emissions (Stanier et al., 2004), but not for Atlanta, which shows a strong organic signature in the growth rate (Kuang et al., 2009). In the model, St. Louis and Po Valley appear to be almost equally split between sulfuric acid and organics. Recent observations in the Po Valley suggest a larger contribution of organics than predicted by the model (Paasonen et al., 2010), although these measurements refer to three case studies with very high growth rates (9.5 nm $h^{-1}$). Though we cannot make definitive statements without additional data, it appears as if the model might underpredict organic condensation in at least some locations, Atlanta in particular. It is possible that a missing source of SOA is potentially causing this underprediction However, the model does not underpredict organic condensation at Hyytiälä, which is the only location where we can make a valid comparison. Organic condensation has been shown to contribute up to 90 % of growth rates at Mexico City (Smith et al., 2008), a level that is not achieved in any of our 5 test locations.

### 3.4 Estimating multi-day survival probabilities

Although it is difficult to assess multi-day survival probabilities in measured nucleation events due to changing air masses, in this section we describe our approach and results to making mutli-day survival probability estimates. As described in Sect. 2.5.4, we present three cases for a multi-day growth and survival of nucleated particles. Our lower bound case is simply the single-day limitation, described in previous sections, which implicitly assumes no further growth after the first day. The upper bound estimate involves assuming all particles that survive the first day become CCN (CN50 or CN100) no matter what size they reached during the first day. The middle estimate, or the partial survival estimate, takes the 25–100 nm growth rates and end-of-day coagulational scavenging rates and extends them indefinitely until the particles are lost. The median survival probabilities for the model simulations and the observations are shown in Table 6. At two of the sites (HYY and SPC), the upper bound on survival probability is as high as ∼ 30 %. The partial survival estimates have an average of about 11 %





ACPD
12, 11765–11822, 2012



across the five sites, but can be as low as 5 % (STL) and as high as 25 % (SPC). In Sect. 3.5, we look at how these survival probabilities translate to CCN formation, and attempt to discern what is driving the survival probabilities – condensational growth or coagulational scavenging.

### 3.5 Contribution to CCN concentrations

Figure 12 shows the impact that boundary layer nucleation and growth events have on global CCN in one year. Figure 12a shows the absolute number of particles 50 nm and larger added by nucleation events ($CN50_{nuc}$), in $cm^{-3}$, calculated according to Eq. (8). Figure 12b shows the absolute number of particles larger than 100 nm added by nucleation ($CN100_{nuc}$). These two quantities are proxies for CCN concentration in the absence of more information on aerosol composition and atmospheric conditions. These two diameter cutoffs were chosen and justified in Sect. 2.5.4. The values of the bars represent the total survival estimate of the contribution of the CCN budget to nucleation, where growth and loss occur beyond one day at a fixed rate. The lower bound on the uncertainty bars in Fig. 12 represent the estimates for CCN from nucleation using the single-day assumptions (e.g. the assumptions used for model-measurement comparison in Figs. 5–9). The upper bound estimate uses the "total survival" case in which all particles that surive the first day of growth will become CCN ($CN50_{nuc}$ or $CN100_{nuc}$), no matter their final size at the end of the day. Looking at the observations alone for the partial survival case (red bars and percentages), atmospheric nucleation events can have mixed impacts on CCN concentrations. When CN50 is the CCN proxy (Fig. 12a), nucleation can contribute as much as 55 % (HYY) to the total CCN budget. However, at Po Valley, a more polluted site, $CN50_{nuc}$ only represents about 6 % of the observed total CN50. As expected, at Hyytiälä nucleation has a strong influence on the total CN50. However, when considering the 100 nm threshold ($CN100_{nuc}$, Fig. 12b), the impact of nucleation on CCN is much smaller. Hyytiälä again shows a strong nucleation signature in CCN concentrations with about 14 % of the CN100 coming from nucleation events. Every other site has a CCN contribution below this 14 % and Atlanta, which has





ACPD
12, 11765–11822, 2012



a low $CN50_{nuc}$ percentage, also has the lowest $CN100_{nuc}$ at 2 %. Tables S1 and S2 in the Supplement show the absolute particle numbers at each size threshold ($cm^{-3}$). Additionally, we show the average CN50 or CN100 for nucleation days only. At most sites, CN50 and CN100 are roughly 5–40 % lower on nucleation days only, meaning that the percent nucleation contribution is higher on these days. Nucleation thus may be a more important source of particle number on cleaner days.

Despite the myriad of different inputs which are all subject to biases, the modeled number concentrations (Fig. 12) seem to be in fairly good agreement with measurements (nearly always within a factor of 2). We note that assuming a CCN lifetime of 7 days for the observations influences our comparison results and leads to some uncertainty. As is expected from the $J_{50}$ and $J_{100}$ formation rates (Figs. 5d, f and 9d, f), number of CCN formed in nucleation and growth events are generally overpredicted by the model. An exception to this is $CN50_{nuc}$ at Pittsburgh, which showed higher measured formation rates than the model predicted. As described in Sect. 2.5.4, these results are not senstive to timing of nucleation bursts due to averaging of formation rates in the CCN calculation over a fixed amount of time. Our $CN50_{nuc}$ results can be interpreted as another upper limit on the contribution of nucleation to CCN in our model, as particles sized below 50 nm are not likely to activate to CCN.

The partial and total survival estimates shown in Fig. 12 (middle estimate and upper uncertainty bar) imply that multi-day growth is indeed an important factor when considering nucleation contribution to CCN. However, as previously noted, ambient observations of multi-day nucleation events are often not reliable because of shifts in the weather patterns and air masses above the point of measurement. Without reliable data to compare against, these single day estimates are most useful for model-measurement comparison, but are also a decent rough estimate of the impact of a year of nucleation events on aerosol number concentrations. Nonetheless, based on results in Fig. 12, we find the contributions of nucleation to be higher, particularly for $CN100_{nuc}$, when multi-day events are considered.





ACPD
12, 11765–11822, 2012



Figures 5–9 show that many of the single-day median survival probabilities are quite low, ranging from about 1 to 9 %. Similarly, the majority of the CCN formation distributions ($J_{50}$ and $J_{100}$) span a range too small to cause large contributions to the CCN budget. Only the upper tail of the distributions (for example, the upper 20 % of Fig. 6f) contain high enough values (approximately 0.02 to 0.1 $cm^{-3} s^{-1}$) that will cause a significant impact on the CCN budget for each site. Based on the single-day definition of the CCN formation rates, these new particle formation events must be days with high nucleation rate ($J_3$), high survival probability, and high growth rate. However, with the partial survival estimate, this does not necessarily have to be the case. To answer quantitatively what is different about these CCN-producing new particle formation events in the partial survival case, we isolate the ten events with the highest CCN formation rate ($J_{100}$) at San Pietro Capofiume (SPC) and Hyytiälä (HYY). We hypothesize that CCN-producing nucleation days (those days with high $J_{100}$) must correlate with days of high growth but not necessarily days with low coagulational scavenging. We find that the ten events in the partial survival case with the highest CCN formation rates also have the ten highest survival probabilities to 100 nm, although the ten events are not ordered identically with respect to both quantities. Among the ∼ 100–150 observed nucleation events, a top CCN formation day always corresponded with a strong growth rate of at least 8 $nm\,h^{-1}$, or the 80th percentile of the growth rate distribution. Conversely, the coagulation sink corresponding to the top ten CCN producing events were spread out over the entire range of the coagulation sink distribution, ranging from around $10^{-5}$ to $10^{-3}\,s^{-1}$. The top CCN producing days included both the 7th highest and 10th lowest coagulation sinks at Po Valley, suggesting that CCN production is more dependent on condensational growth and somewhat less dependent on coagulational scavenging.

## 4 Conclusions

We have presented a novel approach for evaluating aerosol models against observations of boundary layer nucleation, growth and CCN formation. Despite limitations in





ACPD
12, 11765–11822, 2012



the nucleation and SOA parameterizations used in the model, we find that the global model, GEOS-Chem-TOMAS, does an acceptable job of reproducing observed boundary layer nucleation and growth events and their contribution to the CCN budget at the locations used in this study. The methodology presented for analyzing size distribution data applies to both measured and modelled size distribution output, and should be a useful tool for future studies. It builds on earlier methods presented in Dal Maso et al. (2004) and survival probability analysis in Pierce and Adams (2007), Kuang et al. (2009), and Kerminen et al. (2005). In addition, we have advanced the analysis performed by these previous authors by (1) analyzing longer datasets to get a climatology of nucleation-relevant parameters and (2) estimating the net impact of nucleation and growth on the CCN budget and CCN concentrations (Eq. 8). Together, these steps allow for a broader examination of nucleation events within the context of global CCN concentrations. We apply the method to 5 datasets and corresponding model runs with two sets of commonly used nucleation parameterizations.

A challenge in applying this method is that the growth rate is generally insufficient for the nucleation mode to reach CCN sizes on the same day, and growth to CCN sizes on subsequent days is rarely measured by observations at fixed ground sites. Although individual nucleation events can grow quickly enough ($GR > 10\,nm\,h^{-1}$) to form CCN on the same day, these events are somewhat rare as median growth rates are typically 2 to $4\,nm\,h^{-1}$. We address this problem in several ways. First, when CCN are formed on the same day, we quantify this as the contribution from "single-day nucleation and growth events". Second, for events when the nucleation mode does not reach CCN sizes on the same day, we estimate the eventual contribution to CCN formation by extrapolating the final coagulation sink and growth rates and allowing particles as much time for survival to 50 or 100 nm as they need (partial survival case). Fourth, we consider an extreme case (total survival) in which all particles that survive to the end of the first day are assumed to eventually form CCN, neglecting coagulation losses on subsequent days.





ACPD
12, 11765–11822, 2012



Looking at the observations alone, single-day nucleation and growth events contribute only marginally (less than 3 %) to the total CN100 budget. When multi-day growth is accounted for using the partial survival estimate, nucleation accounts for 2–14 % of the observed CN100 concentrations, depending on the site. When the total survival case is used to represent multi-day growth, we find that the nucleation contribution to CN100 can range from about 7–80 %, although this case is considered unrealistically high.

As expected, nucleation is relatively more important to the budget of smaller particles. Results for observed $CN50_{nuc}$ varied from site to site but were significantly larger than $CN100_{nuc}$. At two of the five sites (HYY and SPC), single-day nucleation and growth contributed significantly (40 to 70 %) to the total CN50 budget but was less than 10 % at the other three sites. For the partial survival case, nucleation and growth contributed as much as 55 % to the CN50 budget.

Median and mean survival probabilities to 100 nm are no more than a few percent in the model and the measurements for the single-day estimate. Likewise, CCN formed from nucleation ($CN100_{nuc}$) rarely exceeds 50 particles $cm^{-3}$ when the 100 nm cut-off is considered, but can contribute almost 1000 $cm^{-3}$ of 50 nm and larger particles ($CN50_{nuc}$). When considering multi-day growth (partial survival case), nucleation can contribute as many as 250–750 particles $cm^{-3}$ to the CN100 budget and 500–2000 particles $cm^{-3}$ to the CN50 budget.

For the purposes of model evaluation, we can only rely on the single-day estimates due to data limitations. Nevertheless, we believe that one day of measurement is enough to evaluate the model growth and loss processes (specifically organic condensational growth) that deterimine survival probability. If modeled growth and survival probability is well represented during the first nucleation day, it seems reasonable to assume that the same processes are accurately modeled on subsequent days.

Model predictions of quantities such as event frequency, nucleation rate, growth rate, and particle survival to CCN are within a factor of 2 to 3 (median values for the various sites) when compared to quantities inferred directly from observations. More often,





ACPD
12, 11765–11822, 2012



biases are within 50 % (for example, growth rates at Pittsburgh and Hyytiälä). Rarely, factor of 5 or larger discrepancies are observed in medians or means, as is the case with nucleation rates ($J_3$) at Atlanta and St. Louis. Growth rates were shown to be mostly dominated by organic species in both the model and the measurements at Hyytiälä. Condensation and coagulation sinks were underpredicted in the model, although not by a large enough amount to significantly impact the nucleation metric calculations. Given the gaps in our knowledge of nucleation and secondary organic aerosol, the modelled aerosol dynamics, SOA treatment, and nucleation theories perform reasonably well. Most model quantities' biases seem to be more often positive values than negative, with 15 out of 20 of the ternary and activation $CN50_{nuc}$ and $CN100_{nuc}$ comparisons resulting in model overpredictions.

The overall success of the model does not imply that the current parameterizations are accurate representations of the real chemistry, only that the model tends to get an acceptable result on average. A better understanding of the nucleation mechanism should, in principle, lead to better model skill. Model predictions may benefit from fortuitous "error cancelling". For example, the model may underestimate how much secondary organic material is available for condensation, but we treat secondary organic aerosol as non-volatile, which maximizes how much material will remain in the condensed phase and cause particles to grow (Riipinen et al., 2011). Additionally, we tested the hypothesis that condensation growth wields a bigger influence on particle survival. We find that days with high CCN formation rates are generally days with high condensational growth rates rather than days with low coagulation sinks.

Because the model accuracy was found to be reasonable, our results provide justification for the use of global models as tools for assessing the role of nucleation in the particle number and CCN budgets. We leave improved CCN contribution estimates and sensitivity studies for future work, which can now utilize the tested and evaluated GEOS-Chem-TOMAS global aerosol model. The generality of our conclusions would benefit from more detailed measurements in many parts of the atmosphere. Future modelling studies will especially benefit from long-term nucleation observations at





ACPD
12, 11765–11822, 2012



rural locations, which provide ideal test conditions for coarse resolution global aerosol models. Lastly, since these results depend on long-term ground observations, we reiterate that the relatively models contributions derived here reflect only the effect of nucleation and growth in the boundary layer. Models (Pierce et al., 2009b) and observations (Clarke et al., 1999) suggest that nucleation is frequent in the free troposphere and that they may contribute more to CCN than boundary layer nucleation (Merikanto et al., 2009).

**Supplementary material related to this article is available online at: http://www.atmos-chem-phys-discuss.net/12/11765/2012/acpd-12-11765-2012-supplement.pdf.**

*Acknowledgements.* This research was pursued with funds from the US Environmental Protection Agency under EPA Agreement RD-83337401-0. We would like to thank the Markku Kulmala research group for access to data (HYY). We would also like to thank Peter McMurry (ATL, STL), Maria Cristina Facchini (SPC), and Spyros Pandis (PGH) for access to their datasets. We also thank Peter McMurry and Stefano Decesari for helpful comments on the manuscript. Finally, we would like to thank Tuuka Petäjä for the sulfuric acid measurements at Hyytiälä.

## References

Adams, P. J. and Seinfeld, J. H.: Predicting global aerosol size distributions in general circulation models, J. Geophys. Res.-Atmos., 107, 4370, doi:10.1029/2001jd001010, 2002.

Albrecht, B.: Aerosols, cloud microphysics, and fractional cloudiness, Science, 245, 1227–1230, doi:10.1126/science.245.4923.1227, 1989.

Auvray, M. and Bey, I.: Long-range transport to Europe: seasonal variations and implications for the European ozone budget, J. Geophys. Res., 110, D11303, doi:10.1029/2004JD005503, 2005.





ACPD

12, 11765–11822, 2012



Ball, S. M., Hanson, D. R., Eisele, F. L., and McMurry, P. H.: Laboratory studies of particle nucleation: initial results for $H_2SO_4$, $H_2O$, and $NH_3$ vapors, J. Geophys. Res., 104, 23709–23718, doi:10.1029/1999JD900411, 1999.

Berndt, T., Böge, O., Stratmann, F., Heintzenberg, J., and Kulmala, M.: Rapid formation of sulfuric acid particles at near-atmospheric conditions, Science, 307, 698–700, doi:10.1126/science.1104054, 2005.

Bey, I., Jacob, D. J., Yantosca, R. M., Logan, J. A., Field, B. D., Fiore, A. M., Li, Q. B., Liu, H. G. Y., Mickley, L. J., and Schultz, M. G.: Global modeling of tropospheric chemistry with assimilated meteorology: model description and evaluation, J. Geophys. Res., 106, 23073–23095, 2001.

Bzdek, B. R., Ridge, D. P., and Johnston, M. V.: Amine exchange into ammonium bisulfate and ammonium nitrate nuclei, Atmos. Chem. Phys., 10, 3495–3503, doi:10.5194/acp-10-3495-2010, 2010.

Clarke, A. D., Eisele, F., Kapustin, V. N., Moore, K., Tanner, D., Mauldin, L., Litchy, M., Lienert, B., Carroll, M. A., and Albercook, G.: Nucleation in the equatorial free troposphere: favorable environments during PEM-Tropics, J. Geophys. Res., 104, 5735–5744, doi:10.1029/98JD02303, 1999.

Dal Maso, M., Kulmala, M., Lehtinen, K. E. J., Mäkelä, J. M., Aalto, P., and O'Dowd, C. D.: Condensation and coagulation sinks and formation of nucleation mode particles in coastal and boreal forest boundary layers, J. Geophys. Res., 107, 8097, doi:10.1029/2001JD001053, 2002.

Dal Maso, M., Kulmala, M., Riipinen, I., Wagner, R., Hussein, T., Aalto, P. P., and Lehtinen, K. E. J.: Formation and growth of fresh atmospheric aerosols: eight years of aerosol size distribution data from SMEAR II, Hyytiala, Finland, Boreal Env. Res., 10, 323–336, 2005.

Donahue, N. M., Robinson, A. L., Stanier, C. O., and Pandis, S. N.: Coupled partitioning, dilution, and chemical aging of semivolatile organics, Env. Sci. Tech., 40, 2635–2643, doi:10.1021/es052297c, 2006.

Erupe, M. E., Benson, D. R., Li, J., Young, L.-H., Verheggen, B., Al-Refai, M., Tahboub, O., Cunningham, V., Frimpong, F., Viggiano, A. A., and Lee, S.-H.: Correlation of aerosol nucleation rate with sulfuric acid and ammonia in Kent, Ohio: an atmospheric observation, J. Geophys. Res., 115, D23216, doi:10.1029/2010JD013942, 2010.

Facchini, M. C., Mircea, M., Fuzzi, S., and Charlson, R. J.: Cloud albedo enhancement by surface-active organic solutes in growing droplets, Nature, 401, 257–259, 1999.





ACPD
12, 11765–11822, 2012



Gagné, S., Laakso, L., Petäjä, T., Kerminen, V., and Kulmala, M.: Analysis of one year of ion DMPS data from the SMEAR II station, Finland, Tellus B, 60, 318–329, doi:10.1111/j.1600-0889.2008.00347.x, 2008.

Gagné, S., Nieminen, T., Kurtén, T., Manninen, H. E., Petäjä, T., Laakso, L., Kerminen, V.-M., Boy, M., and Kulmala, M.: Factors influencing the contribution of ion-induced nucleation in a boreal forest, Finland, Atmos. Chem. Phys., 10, 3743–3757, doi:10.5194/acp-10-3743-2010, 2010.

Gong, Y., Hu, M., Cheng, Y., Su, H., Yue, D., Liu, F., Wiedensohler, A., Wang, Z., Kalesse, H., Liu, S., Wu, F., Xiao, K., Mi, P., and Zhang, Y.: Competition of coagulation sink and source rate: new particle formation in the Pearl River Delta of China, Atmos. Environ., 44, 3278–3285, doi:10.1016/j.atmosenv.2010.05.049, 2010.

Guenther, A., Karl, T., Harley, P., Wiedinmyer, C., Palmer, P. I., and Geron, C.: Estimates of global terrestrial isoprene emissions using MEGAN (Model of Emissions of Gases and Aerosols from Nature), Atmos. Chem. Phys., 6, 3181–3210, doi:10.5194/acp-6-3181-2006, 2006.

Hand, J. L., Kreidenweis, S. M., Sherman, D. E., Collett Jr., J. R., Hering, S. V., Day, D. E., and Malm, W. C.: Aerosol size distributions and visibility estimates during the big bend regional aerosol and visibility observational (BRAVO) study, Atmos. Environ., 36, 5043–5055, doi:10.1016/S1352-2310(02)00568-X, 2002.

Jaatinen, A., Hamed, A., Joutsensaari, J., Mikkonen, S., Birmili, W., Wehner, B., Spindler, G., Wiedensohler, A., Decesari, S., Mircea, M., Facchini, M. C., Junninen, H., Kulmala, M., Lehtinen, K. E. J., and Laaksonen, A.: A comparison of new particle formation events in the boundary layer at three different sites in Europe, Boreal Env. Res., 14, 481–498, 2009.

Jung, J., Fountoukis, C., Adams, P. J., and Pandis, S. N.: Simulation of in situ ultrafine particle formation in the Eastern United States using PMCAMx-UF, J. Geophys. Res., 115, D03203, doi:10.1029/2009JD012313, 2010.

Kanakidou, M., Seinfeld, J. H., Pandis, S. N., Barnes, I., Dentener, F. J., Facchini, M. C., Van Dingenen, R., Ervens, B., Nenes, A., Nielsen, C. J., Swietlicki, E., Putaud, J. P., Balkanski, Y., Fuzzi, S., Horth, J., Moortgat, G. K., Winterhalter, R., Myhre, C. E. L., Tsigaridis, K., Vignati, E., Stephanou, E. G., and Wilson, J.: Organic aerosol and global climate modelling: a review, Atmos. Chem. Phys., 5, 1053–1123, doi:10.5194/acp-5-1053-2005, 2005.

Kazil, J., Stier, P., Zhang, K., Quaas, J., Kinne, S., O'Donnell, D., Rast, S., Esch, M., Ferrachat, S., Lohmann, U., and Feichter, J.: Aerosol nucleation and its role for clouds and





ACPD
12, 11765–11822, 2012



Earth's radiative forcing in the aerosol-climate model ECHAM5-HAM, Atmos. Chem. Phys., 10, 10733–10752, doi:10.5194/acp-10-10733-2010, 2010.
Kerminen, V.-M. and Kulmala, M: Analytical formulae connecting the "real" and the "apparent" nucleation rate and the nuclei number concentration for atmospheric nucleation events, J. Aerosol Sci., 33, 609–622, doi:10.1016/S0021-8502(01)00194-X, 2002.
Kerminen, V.-M., Lihavainen, H., Komppula, M., Viisanen, Y., and Kulmala, M.: Direct observational evidence linking atmospheric aerosol formation and cloud droplet activation, Geophys. Res. Lett., 32, L14803, doi:10.1029/2005GL023130, 2005.
Kuang, C., McMurry, P. H., McCormick, A. V., and Eisele, F. L.: Dependence of nucleation rates on sulfuric acid vapor concentration in diverse atmospheric locations, J. Geophys. Res., 113, D10209, doi:10.1029/2007JD009253, 2008.
Kuang, C., McMurry, P. H., and McCormick, A. V.: Determination of cloud condensation nuclei production from measured new particle formation events, Geophys. Res. Lett., 36, L09822, doi:10.1029/2009GL037584, 2009.
Kulmala, M., Pirjola, L., and Makela, J. M.: Stable sulphate clusters as a source of new atmospheric particles, Nature, 404, 66–69, doi:10.1038/35003550, 2000.
Kulmala, M., Vehkamaki, H., Petaja, T., Dal Maso, M., Lauri, A., Kerminen, V. M., Birmili, W., and McMurry, P. H.: Formation and growth rates of ultrafine atmospheric particles: a review of observations, J. Aerosol Sci., 35, 143–176, doi:10.1016/j.jaerosci.2003.10.003, 2004.
Kulmala, M., Riipinen, I., Sipilä, M., Manninen, H. E., Petäjä, T., Junninen, H., Maso, M. D., Mordas, G., Mirme, A., Vana, M., Hirsikko, A., Laakso, L., Harrison, R. M., Hanson, I., Leung, C., Lehtinen, K. E., and Kerminen, V. M.: Toward direct measurement of atmospheric nucleation, Science, 318, 89–92, doi:10.1126/science.1144124, 2007.
Kurtén, T., Loukonen, V., Vehkamäki, H., and Kulmala, M.: Amines are likely to enhance neutral and ion-induced sulfuric acid-water nucleation in the atmosphere more effectively than ammonia, Atmos. Chem. Phys., 8, 4095–4103, doi:10.5194/acp-8-4095-2008, 2008.
Laakso, L., Gagné, S., Petäjä, T., Hirsikko, A., Aalto, P. P., Kulmala, M., and Kerminen, V.-M.: Detecting charging state of ultra-fine particles: instrumental development and ambient measurements, Atmos. Chem. Phys., 7, 1333–1345, doi:10.5194/acp-7-1333-2007, 2007.
Lee, Y. H., Chen, K., and Adams, P. J.: Development of a global model of mineral dust aerosol microphysics, Atmos. Chem. Phys., 9, 2441–2458, doi:10.5194/acp-9-2441-2009, 2009.
Mäkelä, J. M., Aalto, P., Jokinen, V., Pohja, T., Nissinen, A., Palmroth, S., Markkanen, T., Seitsonen, K., Lihavainen, H., and Kulmala, M.: Observations of ultrafine aerosol particle formation





ACPD
12, 11765–11822, 2012



and growth in boreal forest, Geophys. Res. Lett., 24, 1219–1222, doi:10.1029/97GL00920, 1997.

Makkonen, R., Asmi, A., Korhonen, H., Kokkola, H., Järvenoja, S., Räisänen, P., Lehtinen, K. E. J., Laaksonen, A., Kerminen, V.-M., Järvinen, H., Lohmann, U., Bennartz, R., Feichter, J., and Kulmala, M.: Sensitivity of aerosol concentrations and cloud properties to nucleation and secondary organic distribution in ECHAM5-HAM global circulation model, Atmos. Chem. Phys., 9, 1747–1766, doi:10.5194/acp-9-1747-2009, 2009.

Manninen, H. E., Nieminen, T., Riipinen, I., Yli-Juuti, T., Gagné, S., Asmi, E., Aalto, P. P., Petäjä, T., Kerminen, V.-M., and Kulmala, M.: Charged and total particle formation and growth rates during EUCAARI 2007 campaign in Hyytiälä, Atmos. Chem. Phys., 9, 4077–4089, doi:10.5194/acp-9-4077-2009, 2009.

Merikanto, J., Napari, I., Vehkamäki, H., Anttila, T., and Kulmala, M.: New parameterization of sulfuric acid-ammonia-water ternary nucleation rates at tropospheric conditions, J. Geophys. Res., 112, D15207, doi:10.1029/2006JD007977, 2007.

Merikanto, J., Spracklen, D. V., Mann, G. W., Pickering, S. J., and Carslaw, K. S.: Impact of nucleation on global CCN, Atmos. Chem. Phys., 9, 8601–8616, doi:10.5194/acp-9-8601-2009, 2009.

Napari, I., Kulmala, M., and Vehkamaki, H.: Ternary nucleation of inorganic acids, ammonia, and water, J. Chem. Phys., 117, 8418–8425, doi:10.1063/1.1511722, 2002.

Nenes, A., Charlson, R. J., Facchini, M. C., Kulmala, M., Laaksonen, A., and Seinfeld, J. H.: Can chemical effects on cloud droplet number rival the first indirect effect?, Geophys. Res. Lett., 29, 1848, doi:10.1029/2002GL015295, 2002.

Olivier, J. G. J., Bouwman, A. F., Van der Maas, C. W. M., Berdowski, J. J. M., Veldt, C., Bloos, J. P. J., Visschedijk, A. J. H., Zandveld, P. Y. J., and Haverlag, J. L.: Description of EDGAR Version 2.0: A set of global emission inventories of greenhouse gases and ozone-depleting substances for all anthropogenic and most natural sources on a per country basis and on 1 × 1 grid, National Institute of Public Health and the Environment (RIVM) report no. 771060 002, Netherlands Organization for Applied Scientific Research (TNO), 1996.

Paasonen, P., Nieminen, T., Asmi, E., Manninen, H. E., Petäjä, T., Plass-Dülmer, C., Flentje, H., Birmili, W., Wiedensohler, A., Hõrrak, U., Metzger, A., Hamed, A., Laaksonen, A., Facchini, M. C., Kerminen, V.-M., and Kulmala, M.: On the roles of sulphuric acid and low-volatility organic vapours in the initial steps of atmospheric new particle formation, Atmos. Chem. Phys., 10, 11223–11242, doi:10.5194/acp-10-11223-2010, 2010.





ACPD
12, 11765–11822, 2012



Pandis, S. N., Baltensperger, U., Wolfenbarger, J. K., and Seinfeld, J. H.: Inversion of aerosol data from the epiphaniometer, J. Aerosol Sci., 22, 417–428, doi:10.1016/0021-8502(91)90002-Y, 1991.

Petäjä, T., Mauldin, III, R. L., Kosciuch, E., McGrath, J., Nieminen, T., Paasonen, P., Boy, M., Adamov, A., Kotiaho, T., and Kulmala, M.: Sulfuric acid and OH concentrations in a boreal forest site, Atmos. Chem. Phys., 9, 7435–7448, doi:10.5194/acp-9-7435-2009, 2009.

Pierce, J. R. and Adams, P. J.: Efficiency of cloud condensation nuclei formation from ultrafine particles, Atmos. Chem. Phys., 7, 1367–1379, doi:10.5194/acp-7-1367-2007, 2007.

Pierce, J. R. and Adams, P. J.: A computationally efficient aerosol nucleation/condensation method: pseudo-steady-state sulfuric acid, Aerosol Sci Tech., 43, 216, doi:10.1080/02786820802587896, 2009a.

Pierce, J. R. and Adams, P. J.: Uncertainty in global CCN concentrations from uncertain aerosol nucleation and primary emission rates, Atmos. Chem. Phys., 9, 1339–1356, doi:10.5194/acp-9-1339-2009, 2009b.

Pierce, J. R., Chen, K., and Adams, P. J.: Contribution of primary carbonaceous aerosol to cloud condensation nuclei: processes and uncertainties evaluated with a global aerosol microphysics model, Atmos. Chem. Phys., 7, 5447–5466, doi:10.5194/acp-7-5447-2007, 2007.

Pierce, J. R., Riipinen, I., Kulmala, M., Ehn, M., Petäjä, T., Junninen, H., Worsnop, D. R., and Donahue, N. M.: Quantification of the volatility of secondary organic compounds in ultrafine particles during nucleation events, Atmos. Chem. Phys., 11, 9019–9036, doi:10.5194/acp-11-9019-2011, 2011.

Raymond, T. M. and Pandis, S. N.: Formation of cloud droplets by multicomponent organic particles, J. Geophys. Res., 108, 4469, 8 pp., doi:10.1029/2003JD003503, 2003.

Riipinen, I., Pierce, J. R., Yli-Juuti, T., Nieminen, T., Häkkinen, S., Ehn, M., Junninen, H., Lehtipalo, K., Petäjä, T., Slowik, J., Chang, R., Shantz, N. C., Abbatt, J., Leaitch, W. R., Kerminen, V.-M., Worsnop, D. R., Pandis, S. N., Donahue, N. M., and Kulmala, M.: Organic condensation: a vital link connecting aerosol formation to cloud condensation nuclei (CCN) concentrations, Atmos. Chem. Phys., 11, 3865–3878, doi:10.5194/acp-11-3865-2011, 2011.

Riipinen, I., Sihto, S.-L., Kulmala, M., Arnold, F., Dal Maso, M., Birmili, W., Saarnio, K., Teinilä, K., Kerminen, V.-M., Laaksonen, A., and Lehtinen, K. E. J.: Connections between atmospheric sulphuric acid and new particle formation during QUEST III-IV campaigns in Heidelberg and Hyytiälä, Atmos. Chem. Phys., 7, 1899–1914, doi:10.5194/acp-7-1899-2007, 2007.





ACPD
12, 11765–11822, 2012



Seinfeld, J. H. and Pandis, S. N.: Atmospheric Chemistry and Physics – From Air Pollution to Climate Change, 2nd edn., John Wiley & Sons, 2006.

Sihto, S.-L., Kulmala, M., Kerminen, V.-M., Dal Maso, M., Petäjä, T., Riipinen, I., Korhonen, H., Arnold, F., Janson, R., Boy, M., Laaksonen, A., and Lehtinen, K. E. J.: Atmospheric sulphuric acid and aerosol formation: implications from atmospheric measurements for nucleation and early growth mechanisms, Atmos. Chem. Phys., 6, 4079–4091, doi:10.5194/acp-6-4079-2006, 2006.

Sipilä, M., Berndt, T., Petäjä, T., Brus, D., Vanhanen, J., Stratmann, F., Patokoski, J., Mauldin, R. L., Hyvärinen, A.-P., Lihavainen, H., and Kulmala, M.: The Role of sulfuric acid in atmospheric nucleation, Science, 327, 1243–1246, doi:10.1126/science.1180315, 2010.

Smith, J. N., Dunn, M. J., VanReken, T. M., Iida, K., Stolzenburg, M. R., McMurry, P. H., and Huey, L. G.: Chemical composition of atmospheric nanoparticles formed from nucleation in Tecamac, Mexico: evidence for an important role for organic species in nanoparticle growth, Geophys. Res. Lett., 35, L04808, doi:10.1029/2007GL032523, 2008.

Spracklen, D. V., Carslaw, K. S., Merikanto, J., Mann, G. W., Reddington, C. L., Pickering, S., Ogren, J. A., Andrews, E., Baltensperger, U., Weingartner, E., Boy, M., Kulmala, M., Laakso, L., Lihavainen, H., Kivekäs, N., Komppula, M., Mihalopoulos, N., Kouvarakis, G., Jennings, S. G., O'Dowd, C., Birmili, W., Wiedensohler, A., Weller, R., Gras, J., Laj, P., Sellegri, K., Bonn, B., Krejci, R., Laaksonen, A., Hamed, A., Minikin, A., Harrison, R. M., Talbot, R., and Sun, J.: Explaining global surface aerosol number concentrations in terms of primary emissions and particle formation, Atmos. Chem. Phys., 10, 4775–4793, doi:10.5194/acp-10-4775-2010, 2010.

Spracklen, D. V., Jimenez, J. L., Carslaw, K. S., Worsnop, D. R., Evans, M. J., Mann, G. W., Zhang, Q., Canagaratna, M. R., Allan, J., Coe, H., McFiggans, G., Rap, A., and Forster, P.: Aerosol mass spectrometer constraint on the global secondary organic aerosol budget, Atmos. Chem. Phys., 11, 12109–12136, doi:10.5194/acp-11-12109-2011, 2011.

Stanier, C., Khlystov, A., and Pandis, S. N.: Nucleation events during the Pittsburgh air quality study: description and relation to key meteorological, gas phase, and aerosol parameters, Aerosol Sci. Tech., 38, 253–264, 2004.

Stevens, R. G., Pierce, J. R., Brock, C. A., Reed, M. K., Crawford, J. H., Holloway, J. S., Ryerson, T. B., Huey, L. G., and Nowak, J. B.: Nucleation and growth of sulfate aerosol in coal-fired power plant plumes: sensitivity to background aerosol and meteorology, Atmos. Chem. Phys., 12, 189–206, doi:10.5194/acp-12-189-2012, 2012.





ACPD
12, 11765–11822, 2012



Streets, D. G., Bond, T. C., Carmichael, G. R., Fernandes, S. D., Fu, Q., He, D., Klimont, Z., Nelson, S. M., Tsai, N. Y., Wang, M. Q., Woo, J.-H., and Yarber, K. F.: An inventory of gaseous and primary aerosol emissions in Asia in the year 2000, J. Geophys. Res., 108, 8809, doi:10.1029/2002JD003093, 2003.

Stolzenburg, M. R., McMurry, P. H., Sakurai, H., Smith, J. N., Mauldin III, R. L., Eisele, F. L., and Clement, C. F.: Growth rates of freshly nucleated atmospheric particles in Atlanta, J. Geophys. Res., 110, D22S05, doi:10.1029/2005JD005935, 2005.

Trivitayanurak, W., Adams, P. J., Spracklen, D. V., and Carslaw, K. S.: Tropospheric aerosol microphysics simulation with assimilated meteorology: model description and intermodel comparison, Atmos. Chem. Phys., 8, 3149–3168, doi:10.5194/acp-8-3149-2008, 2008.

Twomey, S. A.: Pollution and cloud albedo, Eos T. Am. Geophys. Un., 58, 797–797, 1977.

Tzivion (Tzitzvashvili), S., Feingold, G., and Levin, Z.: An efficient numerical solution to the stochastic collection equation, J. Atmos. Sci., 44, 3139–3149, doi:10.1175/1520-0469(1987)044<3139:AENSTT>2.0.CO;2, 1987.

Vakkari, V., Laakso, H., Kulmala, M., Laaksonen, A., Mabaso, D., Molefe, M., Kgabi, N., and Laakso, L.: New particle formation events in semi-clean South African savannah, Atmos. Chem. Phys., 11, 3333–3346, doi:10.5194/acp-11-3333-2011, 2011.

Vehkamaki, H., Napari, I., Kulmala, M., and Noppel, M.: Stable ammonium bisulfate clusters in the atmosphere, Phys. Rev. Lett., 93, 148501, doi:10.1103/PhysRevLett.93.148501, 2004.

Vuollekoski, H., Nieminen, T., Paasonen, P., Sihto, S.-L., Boy, M., Manninen, H., Lehtinen, K., Kerminen, V.-M., and Kulmala, M.: Atmospheric nucleation and initial steps of particle growth: numerical comparison of different theories and hypotheses, Atmos. Res., 98, 229–236, doi:10.1016/j.atmosres.2010.04.007, 2010.

Wang, M. and Penner, J. E.: Aerosol indirect forcing in a global model with particle nucleation, Atmos. Chem. Phys., 9, 239–260, doi:10.5194/acp-9-239-2009, 2009.

Weber, R. J., Marti, J., McMurry, P. H., Eisele, F. L., Tanner, D. J., and Jefferson, A.: Measured atmospheric new particle formation rates: implications for nucleation mechanisms, Chem. Eng. Comm., 151, 53–64, 1996.

Wu, Z. J., Hu, M., Yue, D. L.,Wehner, B., and Wiedensohler, A.: Evolution of particle number size distribution in an urban atmosphere during episodes of heavy pollution and newparticle formation, Sci. China Earth Sci., 54, 1772–1778, doi:10.1007/s11430-011-4227-9, 2011.





ACPD
12, 11765–11822, 2012



Yu, F. and Luo, G.: Simulation of particle size distribution with a global aerosol model: contribution of nucleation to aerosol and CCN number concentrations, Atmos. Chem. Phys., 9, 7691–7710, doi:10.5194/acp-9-7691-2009, 2009.

Yu, F. and Turco, R. P.: The size-dependent charge fraction of sub-3-nm particles as a key diagnostic of competitive nucleation mechanisms under atmospheric conditions, Atmos. Chem. Phys., 11, 9451–9463, doi:10.5194/acp-11-9451-2011, 2011.

Zhang, R., Suh, I., Zhao, J., Zhang, D., Fortner, E. C., Tie, X., Molina, L. T., and Molina, M. J.: Atmospheric new particle formation enhanced by organic acids, Science, 304, 1487–1490, doi:10.1126/science.1095139, 2004.

Zhang, Y., Liu, P., Liu, X.-H., Jacobson, M. Z., McMurry, P. H., Fang, Q., Bhave, P. V., Yu, S., and Schere, K. L.: A comparative study of homogeneous nucleation parameterizations, Part II: 3-D model simulations and evaluation, J. Geophys Res., 115, D20213. doi:10.1029/2010JD014151, 2010a.

Zhang, Y., McMurry, P. H., Fang, Q., and Jacobson, M. Z.: A comparative study of homogeneous nucleation parameterizations, Part I: examination and evaluation of the formulations, J. Geophys. Res., 115, D20212, doi:10.1029/2010JD014150, 2010b.





ACPD

12, 11765–11822, 2012



**Table 1.** Locations for model comparison.

| | Simulated year | Meteorological fields | Data reference |
|---|---|---|---|
| Pittsburgh, USA (PGH) | Jul 2001–Jun 2002 | GEOS3 | Stanier et al. (2004) |
| Hyytiälä, Finland (HYY) | Jan 2007–Jan 2008 | GEOS5 | Dal Maso et al. (2004) |
| Atlanta, USA (ATL) | Jan 1999–Jan 2000 | GEOS3 | Woo et al. (2001) |
| St. Louis, USA (STL) | Jan 2002–Jan 2003 | GEOS3 | Qian et al. (2007) |
| San Pietro Capiofume, Italy (SPC) | Apr 2002–Mar 2003 | GEOS3 | Laaksonen et al. (2005) |





ACPD
12, 11765–11822, 2012



**Table 2.** Median values for each metric and each site. O = observed, T = ternary simulation, A = activation simulation.

| | Pittsburgh | | | Hyytiälä | | | Atlanta | | | St. Louis | | | Po Valley | | |
|---|---|---|---|---|---|---|---|---|---|---|---|---|---|---|---|
| | O | T | A | O | T | A | O | T | A | O | T | A | O | T | A |
| $J_3$ ($cm^{-3} s^{-1}$) | 2.2 | 1.7 | 1.6 | 0.7 | 0.8 | 0.8 | 0.6 | 1.1 | 0.2 | 2.8 | 3.5 | 1.8 | 1.6 | 2.5 | 1.1 |
| GR ($nm h^{-1}$) | 2.4 | 2.4 | 2.8 | 2.3 | 2.9 | 3.4 | 2.0 | 2.6 | 3.0 | 3.1 | 4.5 | 3.6 | 4.2 | 4.4 | 4.3 |
| $SP_{50}$ (%) | 39 | 28 | 39 | 60 | 70 | 67 | 42 | 42 | 26 | 42 | 53 | 46 | 28 | 29 | 27 |
| $J_{50}$ ($cm^{-3} s^{-1}$) | 1.7 | 0.7 | 1.3 | 0.1 | 0.4 | 0.3 | 0.3 | 0.4 | 0.1 | 0.1 | 0.7 | 0.2 | 0.7 | 0.9 | 0.5 |
| $SP_{100}$ (%) | 1.1 | 1.3 | 0.8 | 1.8 | 1.8 | 1.7 | 1.1 | 1.0 | 1.4 | 0.5 | 1.0 | 1.2 | 8.9 | 7.1 | 11 |
| $J_{100}$ ($cm^{-3} s^{-1}$) | 0.009 | 0.013 | 0.009 | 0.005 | 0.008 | 0.008 | 0.002 | 0.009 | 0.006 | 0.013 | 0.028 | 0.023 | 0.1 | 0.2 | 0.1 |





ACPD
12, 11765–11822, 2012



**Table 3.** Mean values for each metric for each site, nucleation days only. O = observed, T = ternary simulation, A = activation simulation.

| | Pittsburgh | | | Hyytiälä | | | Atlanta | | | St. Louis | | | Po Valley | | |
|---|---|---|---|---|---|---|---|---|---|---|---|---|---|---|---|
| | O | T | A | O | T | A | O | T | A | O | T | A | O | T | A |
| $J_3$ ($cm^{-3} s^{-1}$) | 4.8 | 1.4 | 1.5 | 0.5 | 1.2 | 1.0 | 0.6 | 2.1 | 0.9 | 7.4 | 3.9 | 2.6 | 5.7 | 3.0 | 2.4 |
| GR ($nm h^{-1}$) | 2.5 | 1.9 | 1.8 | 2.8 | 3.3 | 3.7 | 3.4 | 3.5 | 3.8 | 4.1 | 4.7 | 4.6 | 5.5 | 5.0 | 5.3 |
| $SP_{50}$(%) | 33 | 35 | 32 | 49 | 63 | 59 | 40 | 40 | 30 | 40 | 50 | 50 | 33 | 36 | 31 |
| $J_{50}$ ($cm^{-3} s^{-1}$) | 1.6 | 0.8 | 0.6 | 0.3 | 0.9 | 0.8 | 0.3 | 0.4 | 0.2 | 0.1 | 0.7 | 0.2 | 1.2 | 1.7 | 0.8 |
| $SP_{100}$ (%) | 0.9 | 1.1 | 1.0 | 1.4 | 2.3 | 2.5 | 1.2 | 0.9 | 1.5 | 0.4 | 0.8 | 0.9 | 17 | 15 | 19 |
| $J_{100}$ ($cm^{-3} s^{-1}$) | 0.010 | 0.007 | 0.008 | 0.009 | 0.012 | 0.013 | 0.01 | 0.011 | 0.009 | 0.012 | 0.021 | 0.031 | 0.4 | 0.49 | 0.34 |





ACPD
12, 11765–11822, 2012



**Table 4.** Modelled versus measured log-mean normalized biases (LMNB) for each metric and each site, nucleation days only. T = ternary simulation, A = activation simulation.

| | Pittsburgh | | Hyytiälä | | Atlanta | | St. Louis | | Po Valley | |
|---|---|---|---|---|---|---|---|---|---|---|
| | T | A | T | A | T | A | T | A | T | A |
| $J_3$ | −0.15 | −0.10 | 0.23 | 0.20 | 0.7 | 0.05 | −0.20 | −0.15 | 0.23 | −0.09 |
| GR | −0.03 | −0.02 | 0.04 | 0.06 | 0.04 | 0.06 | 0.10 | 0.08 | 0.19 | 0.14 |
| $SP_{50}$ | 0.07 | 0.08 | 0.10 | 0.02 | 0.09 | 0.11 | 0.10 | 0.15 | −0.14 | 0.17 |
| $J_{50}$ | −0.01 | −0.07 | 0.09 | 0.36 | 0.10 | 0.30 | 0.67 | 0.53 | 0.10 | −0.05 |
| $SP_{100}$ | 0.03 | −0.05 | −0.05 | −0.08 | 0.09 | 0.10 | 0.29 | 0.36 | −0.01 | 0.05 |
| $J_{100}$ | −0.15 | −0.16 | 0.023 | 0.02 | 0.60 | 0.33 | 0.23 | 0.30 | 0.05 | 0.02 |





ACPD
12, 11765–11822, 2012



**Table 5.** Mean values for nucleation event numbers for each site. O = observed, T = ternary simulation, A = activation simulation.

| | Pittsburgh | | | Hyytiälä | | | Atlanta | | | St. Louis | | | Po Valley | | |
|---|---|---|---|---|---|---|---|---|---|---|---|---|---|---|---|
| | O | T | A | O | T | A | O | T | A | O | T | A | O | T | A |
| Number of total events | 109 | 114 | 129 | 107 | 121 | 144 | 108 | 137 | 145 | 102 | 133 | 166 | 145 | 166 | 176 |
| Number of growth events to 50 nm | 42 | 40 | 49 | 39 | 48 | 36 | 25 | 47 | 43 | 24 | 37 | 39 | 65 | 64 | 64 |
| Number of growth events to 100 nm | 9 | 10 | 9 | 19 | 21 | 21 | 17 | 20 | 20 | 17 | 25 | 18 | 53 | 53 | 59 |





ACPD
12, 11765–11822, 2012



**Table 6.** Median survival probabilities (%) to 100 nm for the three multi-day growth assumptions. O = observed, T = ternary simulation, A = activation simulation.

| | Pittsburgh | | | Hyytiälä | | | Atlanta | | | St. Louis | | | Po Valley | | |
|---|---|---|---|---|---|---|---|---|---|---|---|---|---|---|---|
| | O | T | A | O | T | A | O | T | A | O | T | A | O | T | A |
| Single-day only | 1.1 | 1.3 | 0.8 | 1.8 | 1.8 | 1.7 | 1.1 | 1.0 | 1.4 | 0.5 | 1.0 | 1.2 | 8.9 | 7.1 | 11 |
| Partial survival | 8.3 | 9.6 | 8.9 | 9.9 | 11.3 | 12.9 | 9.2 | 9.2 | 8.9 | 4.5 | 5.6 | 5.3 | 19.0 | 18.8 | 25.5 |
| Total survival | 19.3 | 22.0 | 24.2 | 25.4 | 27.0 | 29.7 | 19.1 | 19.9 | 18.9 | 9.2 | 10.3 | 10.0 | 33.0 | 31.4 | 36.8 |





ACPD
12, 11765–11822, 2012



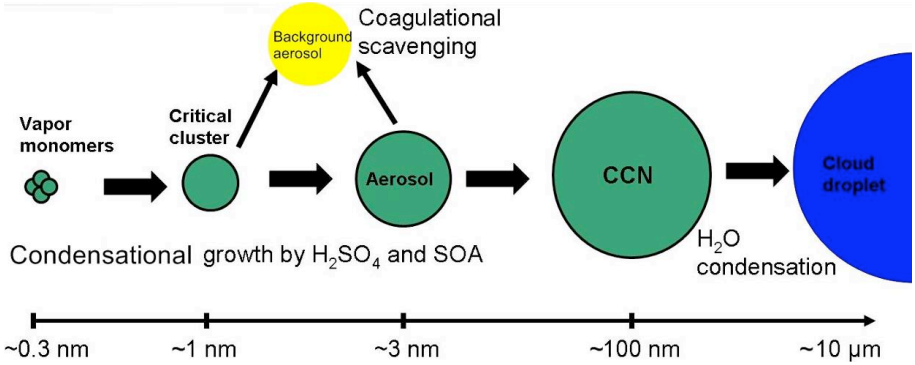


**Fig. 1.** Dynamics of new particle formation from vapour to cloud droplet. The two possible fates for freshly formed atmospheric nuclei are condensational growth (eventually forming CCN) or coagulational scavenging, which results in the loss of the nuclei.





ACPD
12, 11765–11822, 2012



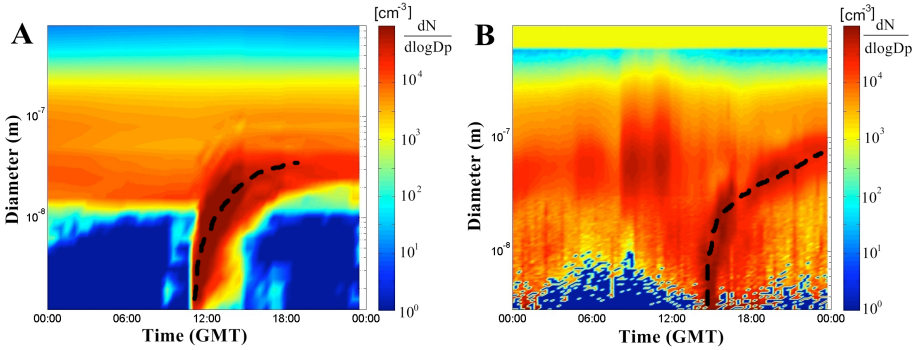


**Fig. 2.** Sample new particle formation events in the model with ternary nucleation ($10^{-5}$ tuning factor) and measurements at Pittsburgh. Contours represent values of the size distribution function plotted against particle diameter in m (ordinate) and time in GMT (abscissa). Dashed line represents the diameter growth trajectory **(A)** Pittsburgh, PA, USA modeled, 16 April, 2002 **(B)** Pittsburgh, measured, 16 April, 2002.





ACPD
12, 11765–11822, 2012



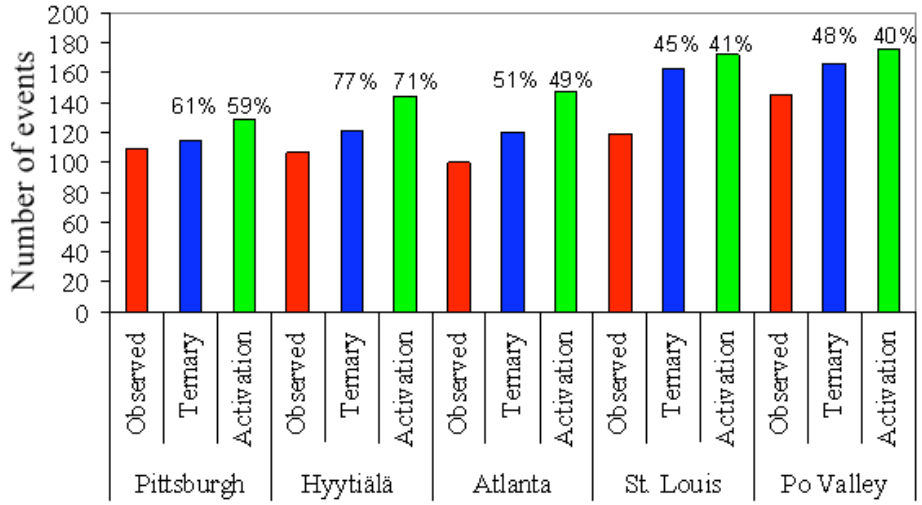


**Fig. 3.** New particle formation event frequency for one year across the five datasets and simulations. Observations are in red, ternary with a $10^{-5}$ tuning factor nucleation simulation is in blue, and activation nucleation simulation is in green. Numbers above the ternary and activation columns represent the percentage of matching events or non-events for the two model cases compared to observations.





ACPD
12, 11765–11822, 2012



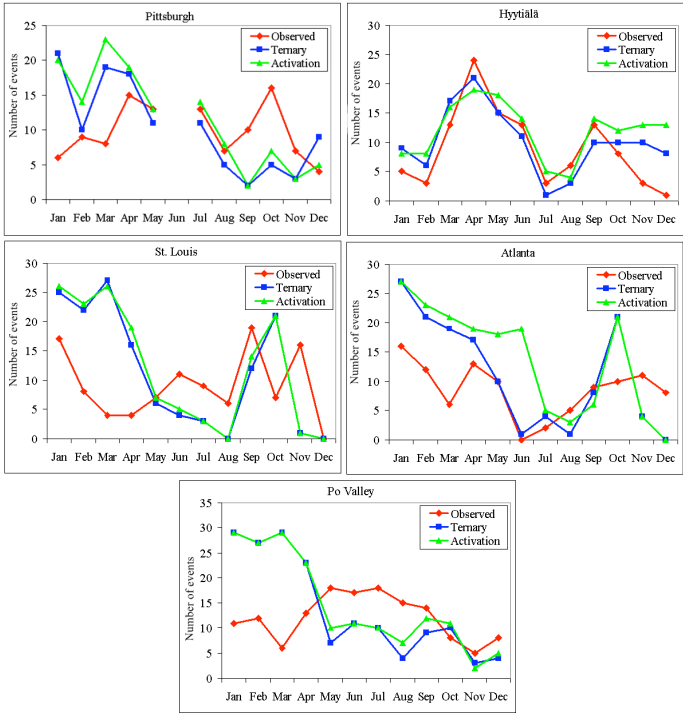


**Fig. 4.** New particle formation event frequency as a function of month for the five datasets and simulations. Observations are in red, ternary nucleation model (with a $10^{-5}$ tuning factor) is in blue, and activation nucleation is in green. Data is missing in June at PGH due to SMPS malfunction.





ACPD
12, 11765–11822, 2012



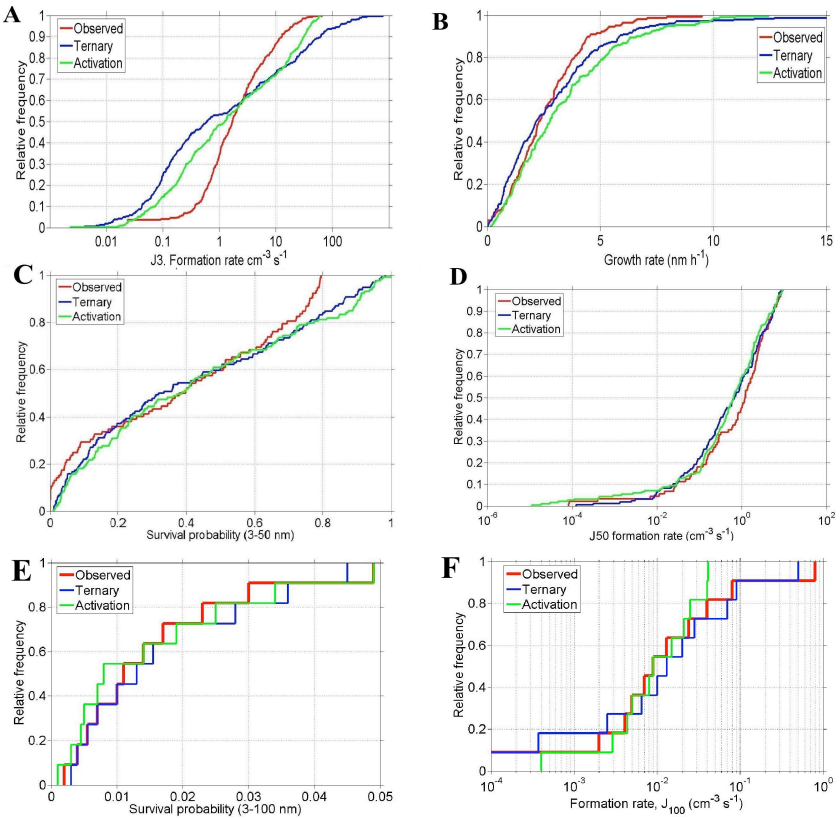


**Fig. 5.** Cumulative distribution function (CDF) of modelled and measured nucleation metrics at Pittsburgh (PGH). Twenty-four hour averaged nucleation rate ($J_3$) is shown in **(A)**, growth rate in **(B)**, survival probability to 50 nm ($SP_{3–50}$) in **(C)**, 50 nm particle formation rate ($J_{50}$) in **(D)**, survival probability to 100 nm ($SP_{3–100}$) in **(E)**, and 100 nm particle formation rate ($J_{100}$) in **(F)**. Descriptive statistics for these distributions can be found in Tables 2–4.





ACPD
12, 11765–11822, 2012



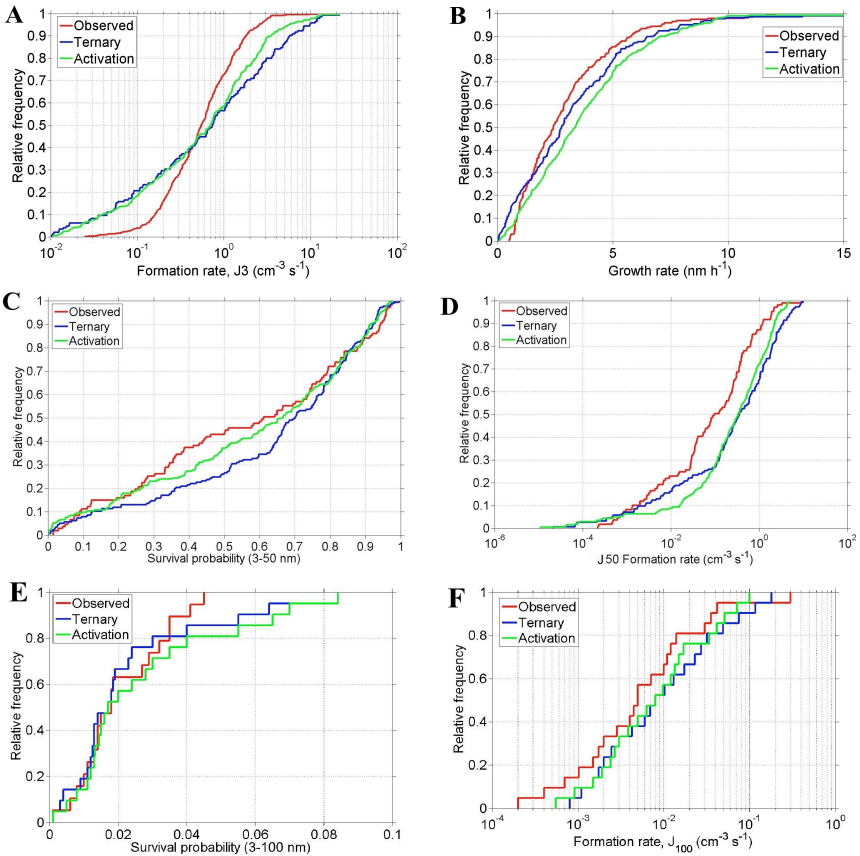


**Fig. 6.** Cumulative distribution function (CDF) of modelled and measured nucleation metrics at Hyytiälä (HYY). Twenty-four hour averaged nucleation rate ($J_3$) is shown in **(A)**, growth rate in **(B)**, survival probability to 50 nm ($SP_{3-50}$) in **(C)**, 50 nm particle formation rate ($J_{50}$) in **(D)**, survival probability to 100 nm ($SP_{3-100}$) in **(E)**, and 100 nm particle formation rate ($J_{100}$) in **(F)**. Descriptive statistics for these distributions can be found in Tables 2–4.





ACPD
12, 11765–11822, 2012



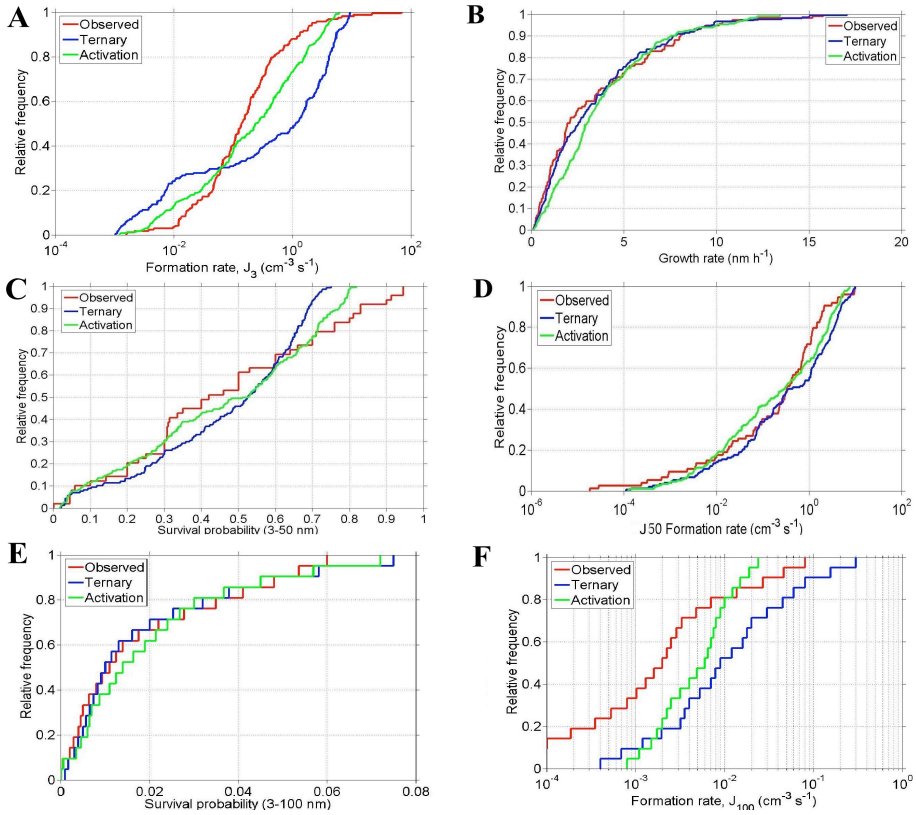


**Fig. 7.** Cumulative distribution function (CDF) of modelled and measured nucleation metrics at Atlanta (ATL). Twenty-four hour averaged nucleation rate ($J_3$) is shown in **(A)**, growth rate in **(B)**, survival probability to 50 nm ($SP_{3-50}$) in **(C)**, 50 nm particle formation rate ($J_{50}$) in **(D)**, survival probability to 100 nm ($SP_{3-100}$) in **(E)**, and 100 nm particle formation rate ($J_{100}$) in **(F)**. Descriptive statistics for these distributions can be found in Tables 2–4.





ACPD
12, 11765–11822, 2012



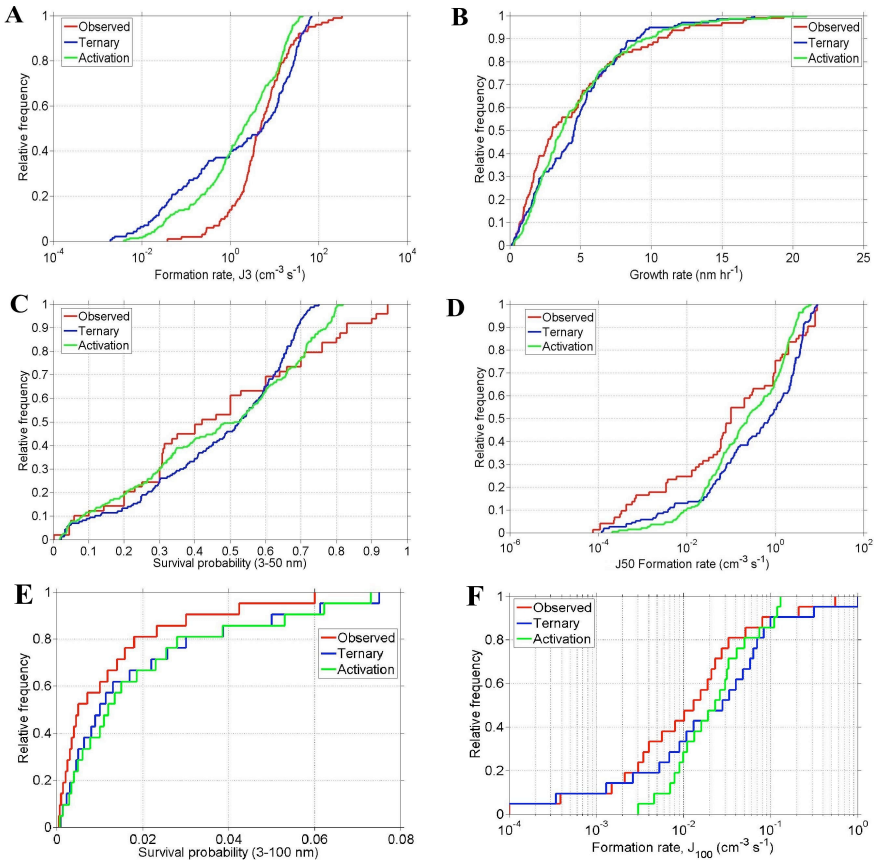


**Fig. 8.** Cumulative distribution function (CDF) of modelled and measured nucleation metrics at St. Louis (STL). Twenty-four hour averaged nucleation rate ($J_3$) is shown in **(A)**, growth rate in **(B)**, survival probability to 50 nm ($SP_{3-50}$) in **(C)**, 50 nm particle formation rate ($J_{50}$) in **(D)**, survival probability to 100 nm ($SP_{3-100}$) in **(E)**, and 100 nm particle formation rate ($J_{100}$) in **(F)**. Descriptive statistics for these distributions can be found in Tables 2–4.





ACPD
12, 11765–11822, 2012



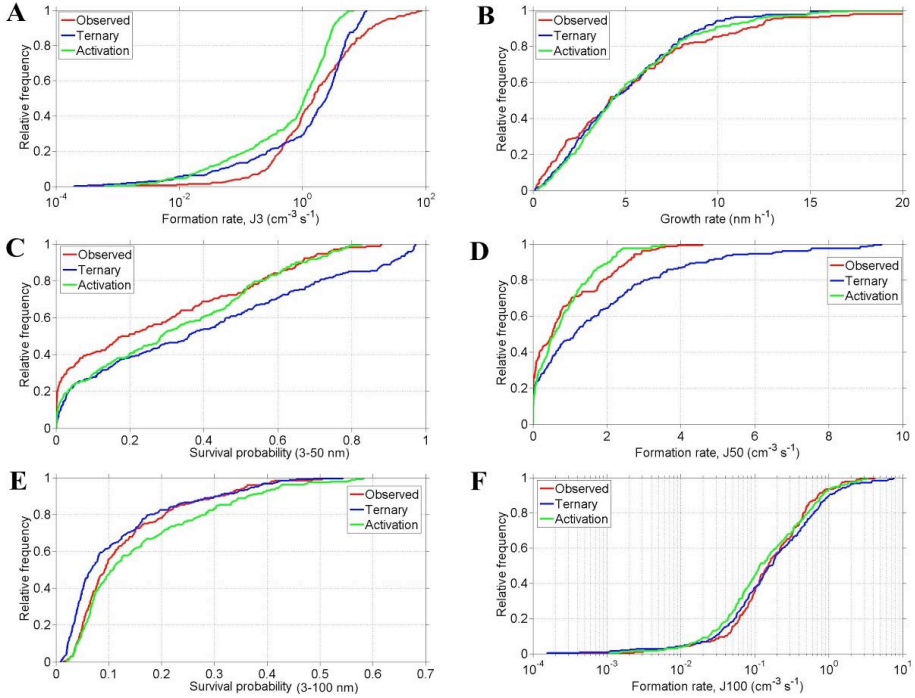


**Fig. 9.** Cumulative distribution function (CDF) of modelled and measured nucleation metrics at San Pietro Capofiume, Po Valley (SPC). Twenty-four hour averaged nucleation rate ($J_3$) is shown in **(A)**, growth rate in **(B)**, survival probability to 50 nm ($SP_{3-50}$) in **(C)**, 50 nm particle formation rate ($J_{50}$) in **(D)**, survival probability to 100 nm ($SP_{3-100}$) in **(E)**, and 100 nm particle formation rate ($J_{100}$) in **(F)**. Descriptive statistics for these distributions can be found in Tables 2–4.





ACPD
12, 11765–11822, 2012



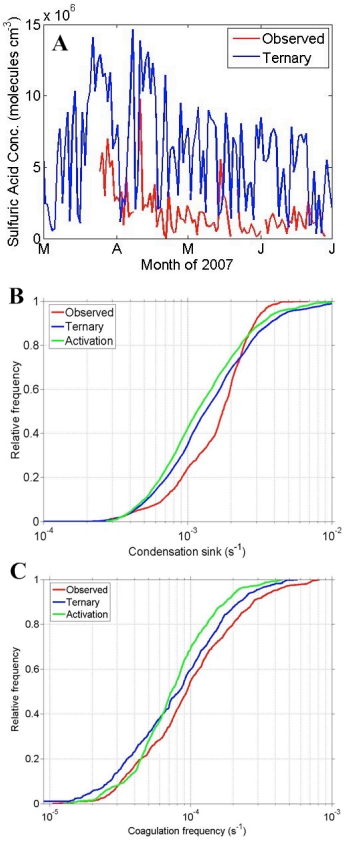


**Fig. 10.** Additional nucleation metrics at Hyytiälä for the ternary (with $10^{-5}$ tuning factor) and activation models and the measurements. **(A)** shows the maximum daily sulfuric acid concentration. **(B)** is a cumulative distribution function (CDF) of modelled and measured condensation sink values. **(C)** shows the CDF of coagulation sink for 3 nm particles.





ACPD
12, 11765–11822, 2012



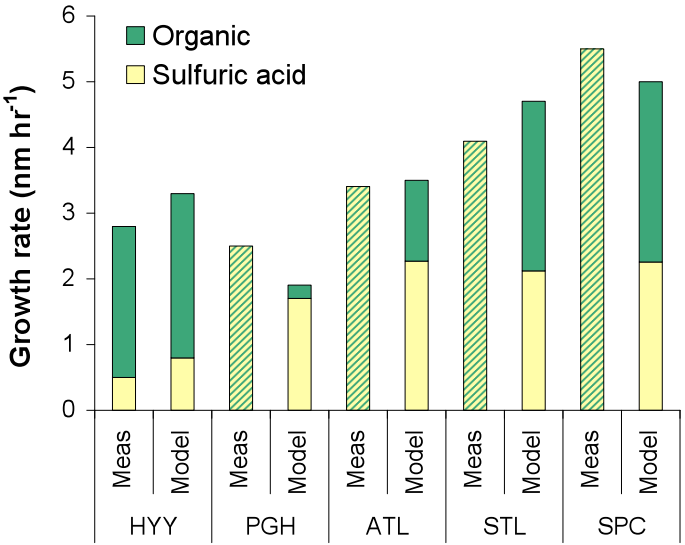


**Fig. 11.** Annually averaged growth rate as a function of condensing vapour chemical species, either low volatility organics or sulfuric acid, for observations and model (ternary nucleation with $10^{-5}$ tuning factor simulation) results at each of the five locations. Green shading represents organic condensation and yellow represents sulfuric acid. Sulfuric acid measurements (and therefore speciation analyses) were only available at Hyytiälä for the simulated time periods. For these sites without measurements, total growth rate is plotted without knowledge of breakdown between condensing vapour (yellow with green shading). Units are in $\mathrm{nm\,h^{-1}}$.





ACPD
12, 11765–11822, 2012



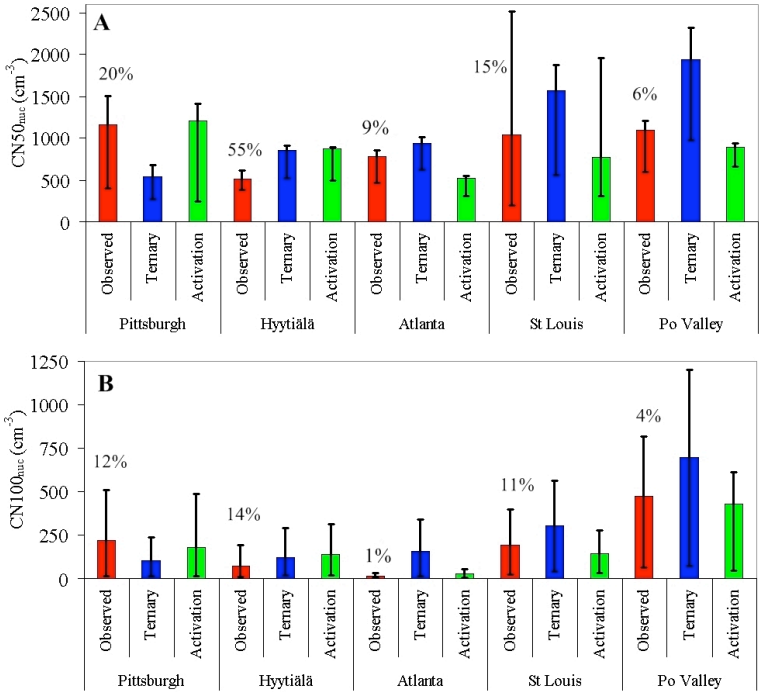


**Fig. 12. (A)** shows the annual-average number concentrations ($cm^{-3}$) of particles 50 nm and larger in diameter attributable to boundary layer new particle formation events and growth ($CN50_{nuc}$). **(B)** shows the same for number concentrations of particles 100 nm and larger in diameter ($CN100_{nuc}$). Error bars represent the limits of the possible contribution based on the lower bound (single-day) and upper bound calculations (total survival). Solid colored bars show the partial survival estimate of contribution to $CCN_{nuc}$, based on extrapolating nucleation parameters into future days to account for multi-day growth (see Sect. 2.5.4 for more details). Numbers above the bars indicate the percentage of nucleation-produced CCN compared to CCN from all sources (measurements only, see text also).





ACPD
12, 11765–11822, 2012